Published in final edited form as:

Cell Rep. 2023 February 28; 42(2): 112037. doi:10.1016/j.celrep.2023.112037.

The selective autophagy adaptor p62/SQSTM1 forms phase condensates regulated by HSP27 that facilitate the clearance of damaged lysosomes via lysophagy

Elizabeth R. Gallagher[1], **Erika L.F. Holzbaur**[1,2,*]

[1]Department of Physiology, University of Pennsylvania Perelman School of Medicine, Philadelphia, PA 19104, USA

[2]Lead contact

SUMMARY

In response to lysosomal damage, cells engage several quality-control mechanisms, including the selective isolation and degradation of damaged lysosomes by lysophagy. Here, we report that the selective autophagy adaptor SQSTM1/p62 is recruited to damaged lysosomes in both HeLa cells and neurons and is required for lysophagic flux. The Phox and Bem1p (PB1) domain of p62 mediates oligomerization and is specifically required for lysophagy. Consistent with this observation, we find that p62 forms condensates on damaged lysosomes. These condensates are precisely tuned by the small heat shock protein HSP27, which is phosphorylated in response to lysosomal injury and maintains the liquidity of p62 condensates, facilitating autophagosome formation. Mutations in p62 have been identified in patients with amyotrophic lateral sclerosis (ALS); ALS-associated mutations in p62 impair lysophagy, suggesting that deficits in this pathway may contribute to neurodegeneration. Thus, p62 condensates regulated by HSP27 promote lysophagy by forming platforms for autophagosome biogenesis at damaged lysosomes.

Graphical Abstract

*Correspondence: holzbaur@pennmedicine.upenn.edu.

AUTHOR CONTRIBUTIONS

E.R.G. and E.L.F.H. devised experiments and wrote the manuscript. E.R.G. performed the experiments and subsequent analysis with supervision by E.L.F.H.

SUPPLEMENTAL INFORMATION

Supplemental information can be found online at https://doi.org/10.1016/j.celrep.2023.112037.

DECLARATION OF INTERESTS

The authors declare no competing interests.

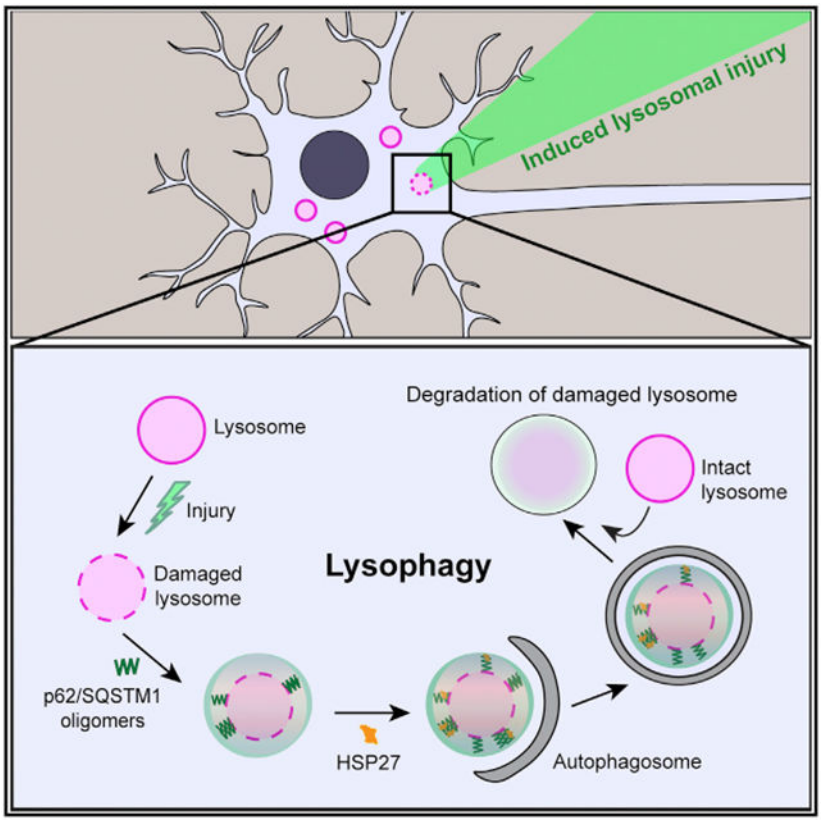

In brief

Gallagher and Holzbaur characterize the requirement for p62/SQSTM1 in the selective autophagy of damaged lysosomes in neurons and HeLa cells. p62 forms phase condensates via an interaction with the small heat shock protein HSP27. Depletion of p62 or HSP27 inhibits clearance of damaged lysosomes, threatening cellular homeostasis.

INTRODUCTION

Lysosomes are the primary degradative organelle in mammalian cells, responsible for the enzymatic digestion and recycling of macromolecules.[1] Lysosomal dysfunction and permeabilization endanger cellular health, risking release of calcium, degradative enzymes, and reactive oxygen species into the cytosol and initiating cell death pathways.[2-6]

Lysosomal dysfunction is particularly injurious to the central nervous system, as shown by the emerging link between disruption of lysosomal health and neurodegenerative disease.[7-11] Disorders linked to lysosomal dysfunction include lysosomal storage disorders, Parkinson's disease, Alzheimer's disease, frontotemporal dementia, and amyotrophic lateral sclerosis (ALS).[8,12,13] Lysosomal rupture has specifically been identified in Niemann-Pick type A, Gaucher's disease, and Parkinson's disease.[14-17] Because lysosomal rupture can be extremely damaging to the cell, quality-control mechanisms are engaged to rescue lysosomal integrity and protect the cell from lysosome-mediated cell death. However, there are few established mechanisms of neuronal lysosomal quality control.[18,19]

Lysosomal quality control begins with an attempt to repair damaged lysosomes via the endosomal sorting complexes required for transport (ESCRT) machinery.[20,21] In the absence of lysosomal repair, ruptured lysosomes are targeted for degradation via selective autophagy, referred to as lysophagy.[20-22] Selective autophagy is a process in which autophagosomes, double-membraned vesicles, form in the cytoplasm to sequester and ultimately degrade cellular cargo.[23-25] Damaged lysosomes can undergo ubiquitin-dependent lysophagy.[20,26-30] The ubiquitination of lysosomal proteins drives the recruitment of selective autophagy adaptors that facilitate the selective engulfment of damaged lysosomes.[20,23,25,28,30] Several adaptors have been identified on the surface of damaged endolysosomes, including NDP52, TAX1BP1, and p62/SQSTM1.[18,28,31-34] Previous work has examined roles for NDP52 and TAX1BP1 in endolysosomal damage response,[18,35] but the role of p62 in lysophagy has remained unclear. p62 is essential for the selective autophagy of protein aggregates (aggrephagy),[25] forming liquid-liquid phase separated condensates.[36,37] p62 condensates also appear to be critical in the Parkin-independent selective autophagy of mitochondria (mitophagy)[38]; however, p62 is not required for Parkin-dependent mitophagy.[39,40] Together, these data suggest that p62 condensates are required for some, but not all, types of selective autophagy, prompting the question whether p62 condensates are required in lysophagy.

Here, we demonstrate that p62 functions as an essential lysophagy adaptor, responding to lysosomal damage in HeLa cells, as well as in human induced pluripotent stem cell (iPSC)-derived neurons and primary rat hippocampal neurons. This response is selective, which we demonstrate using the genetically encoded lysosomal photosensitizer KillerRed to focally damage lysosomes. This response is also essential, because loss of p62 inhibits the autophagic degradation of damaged lysosomes. Loss of p62 self-association prevents its recruitment to damaged lysosomes and impairs engulfment of the organelles by ATG8-positive autophagosomes. Moreover, we find that p62 facilitates the recruitment of the small heat shock protein HSP27. HSP27 is phosphorylated in response to lysosomal damage and, once recruited, maintains the liquid-like state of p62 oligomers to promote lysophagy. ALS-associated mutations in p62 disrupt lysophagy in cellular assays, further implicating defects in lysosomal quality control in neurodegenerative disease. Thus, we propose that p62 facilitates lysophagy via condensate formation that is regulated by HSP27, forming a platform for *de novo* autophagosome biogenesis to rapidly and effectively engulf damaged lysosomes.

RESULTS

p62 is dynamically recruited to damaged lysosomes in HeLa cells

We used lysosomal immunoprecipitation[41] to examine the association of p62 with lysosomes following treatment of HeLa cells with the well-characterized lysomotropic agent L-leucyl-L-leucine methyl ester (LLOMe).[20-22,30,42-45] Cells were either untreated or treated with 1.0 mM LLOMe for 1 h priorto lysosomal immunoprecipitation. We observed significant increases in lysosome-associated FIP200, TAX1BP1, p62, and lipidated mammalian ATG8-family proteins (GABARAP/L1/L2 and LC3B) in LLOMe-treated cells (Figures 1A-1F), indicating that p62 accumulates on damaged lysosomes, along with proteins required for autophagosome biogenesis.

To validate our immunoprecipitation results, we assayed endogenous p62 recruitment to damaged lysosomes using immunofluorescence. Lysosomes were identified as organelles positive for the lysosomal transmembrane protein Lysosomal-associated membrane protein 1 (LAMP1).[46] We observed significant increases in the fraction of lysosomal area occupied by endogenous p62 when treated with 250 or 750 μM LLOMe (ethanol [EtOH]: 1.1% ± 0.43%; 250 μM LLOMe: 20% ± 2.3%; 750 μM LLOMe: 25% ± 0.68%) (Figures 1G and 1H), with no differences in average cellular area of LAMP1 (Figure 1I).[30,33]

Next, we asked whether p62 recruitment represents a broader response to lysosomal injury. We engineered a genetically encoded, lysosomal-membrane-targeted photosensitizer by fusion of KillerRed to the C terminus of LAMP1. LAMP1-KillerRed induces lysosomal injury via local production of reactive oxygen species (ROS) following 561-nm laser irradiation.[47] KillerRed activation resulted in the accumulation of EGFP-p62 on lysosomes marked by LAMP2-BFP within 10 min of injury (Figures 1J-1M) (Video S1). In regions of cells where KillerRed was inactive, we observed no change in EGFP-p62 intensity. Therefore, p62 responds quickly to both cellular-scale lysosomal rupture and focal lysosomal damage in HeLa cells.

Our lysosomal immunoprecipitation results suggested that p62 recruitment coincides with the recruitment of proteins known to be required for autophagosome biogenesis (Figures 1A and 1B). Thus, we wondered whether p62 co-localizes with the well-characterized autophagosome markers, ATG8-family proteins GABARAP/L1/L2, referred herein collectively as GABARAPs. Following LLOMe addition, we observed a significant increase in the recruitment of endogenous GABARAPs to damaged lysosomes (Figures 1N and 1O) and a striking co-localization of p62 with GABARAPs (Figure 1N). In single z-slices, GABARAP can appear as puncta or as rings, where rings are indicative of formed autophagosomes (Figure 1N). We observed that 94% ± 0.49% of GABARAP rings were co-positive for endogenous p62 (Figures 1P and 1Q). Thus, p62 is poised to regulate lysophagy in HeLa cells.

p62 responds to lysosomal damage in human and rat neurons

Lysosomal dysfunction has been implicated in several neurodegenerative diseases, so we asked whether p62 exhibits a similar response to lysosomal damage in neurons. We utilized a well-characterized human iPSC line expressing doxycycline-inducible Neurogenin 2, allowing for efficient differentiation into glutamatergic cortical neurons (i^3Neurons).[48,49] We visualized lysosomes via CRISPR tagging of endogenous LAMP1 with mNeonGreen[48] and observed a significant increase in endogenous p62 recruitment to lysosomes in i^3Neurons treated with 1.0 mM LLOMe for 2 h (EtOH: 4.6% ± 0.49%; LLOMe: 20% ± 1.7%; Figures 2A-2C).

We compared these observations with the recruitment of other autophagy adaptors: TAX1BP1, NDP52, and OPTN. We observed a small but significant enrichment of endogenous TAX1BP1 on lysosomes following LLOMe treatment (EtOH: 2.7% ± 0.30%; LLOMe: 8.5% ± 1.8%) (Figures 2D-2F) in accordance with a previous report.[18] In contrast, we observed no enrichment of endogenous NDP52 or OPTN (Figures 2G-2L) on damaged lysosomes in i^3Neurons.

Next, we asked whether lysosomes recruit p62 following focal lysosomal damage in primary neurons. We expressed LAMP1-KillerRed in primary rat hippocampal neurons and found that KillerRed activation induced EGFP-p62 accumulation on lysosomes labeled by LAMP2-BFP (Figures 2M-2P). EGFP-p62 accumulation was induced within 5 min and was observed only in regions irradiated with the 561-nm laser (Figure 2P) (Video S2). Thus, p62 responds to focal lysosomal damage in primary neurons.

In all, we observe that p62 is robustly and rapidly localized to damaged lysosomes in HeLa cells, human iPSC-derived neurons, and primary rat hippocampal neurons, prompting investigation into the functional significance of p62 in lysophagy.

p62 is necessary and sufficient for lysophagy

To investigate the requirement for p62 in lysophagy, we first needed to develop more effective tools. A number of studies have utilized either the recruitment or clearance of galectins to monitor lysosomal damage or lysophagy.[18-22,28,30,50] Transcriptomic analysis predicts that certain galectins are expressed at low levels in the human central nervous system.[50] Consistent with these transcriptomic data, we observed no detectable expression of galectin-3 on western blots of cell lysates from either mouse cortical neurons or human i^{3}Neurons (Figures S1A and S1B). Galectin-8, however, was expressed in both mouse and human neurons (Figures S1A and S1C).[50] Given the inconsistencies in galectin expression across cell types, we sought a galectin-independent method to rapidly identify damaged lysosomes.

Recent work has demonstrated that LAMTOR2, also referred to as p14, responds to endolysosomal damage following *S. typhimurium* infection.[51] LAMTOR2 is a cytosolic component of the Ragulator complex and regulates cellular metabolism.[52] We observed that LAMTOR2 was expressed in HeLa cells, i^{3}Neurons, and mouse cortical neurons (Figures S1D and S1E), and we found that both GFP-galectin-3 and mCherry-LAMTOR2 were recruited to lysosomes on addition of 750 μM LLOMe, co-localizing with LAMP1-Halo (Figures S1F-S1H) (Video S3). There was no significant difference in the number of mCherry-LAMTOR2 puncta per cell as compared with GFP-galectin-3, suggesting that LAMTOR2 is equivalently capable of rapid translocation to lysosomes (Figures S1G and S1H).

Additionally, we observed that the majority of LAMTOR2-positive puncta (72% ± 3.5%) co-localized with HaloTag-p62 in HeLa cells (Figures S1I-S1K). In rat hippocampal neurons, we observed that LAMTOR2 forms puncta following LLOMe addition (Figures S1L and S1M), and that the majority of LAMTOR2 puncta (80% ± 9.6%) co-localized with EGFP-p62 (Figures S1L and S1N). We also observed that EGFP-p62 formed ring-like structures akin to forming autophagosomes in neurons following LLOMe treatment (Figure S1O).

We used LAMTOR2 to test both the necessity and sufficiency of p62 in lysophagy initiation. To assay for sufficiency, we utilized a well-characterized HeLa cell line lacking the five sequestosome-like autophagy adaptors (p62, TAX1BP1, NBR1, OPTN, and NDP52) referred to as penta-knockout (pentaKO) HeLa cells,[53] focusing on p62, TAX1BP1, and NBR1. Our lysosomal immunoprecipitations identified both p62 and TAX1BP1 associating

with damaged lysosomes (Figures 1A, 1C, and 1D). NBR1 was reported not to be on damaged lysosomes,[33] but NBR1 and p62 have similar domain structures;[54] thus, we also tested the functional role of this adaptor.

To measure sufficiency, we evaluated the recruitment of the endogenous ATG8-family protein LC3B to damaged lysosomes using immunofluorescence. Strikingly, only expression of EGFP-p62 was sufficient to increase LC3B intensity in pentaKO HeLa cells following 2-h treatment with 750 μM LLOMe (Figures 3A, 3B, and S2A). LAMTOR2 recruitment was similar across conditions, indicating that lysosomal damage was induced to a similar extent (Figure S2B), while measurements of EGFP intensity ensured equivalent levels of expression of EGFP-labeled adaptors in these assays (Figure S2C). We assayed the extent by which p62 rescues LC3B recruitment in pentaKO HeLa, and we observed a full rescue to wild-type (WT) levels (Figures S2D-S2F). These data indicate a non-redundant function for p62 in lysophagy, which cannot be replaced by TAX1BP1 or NBR1.

We next evaluated the necessity of p62 using acute depletion of p62 by small interfering RNA (siRNA) knockdown. Depletion of p62 (siRNA #1: 95% ± 1.3% knockdown) (Figures S3A and S3B) decreased lysophagy initiation, measuring the fluorescence intensity of endogenous LC3B at LAMTOR2 puncta after LLOMe treatment (Figures 3C-3E). Therefore, p62 is both necessary and sufficient for lysophagy initiation.

We next assessed whether p62 is required for the degradation of damaged lysosomes. We first asked whether overall autophagic flux is decreased following lysosomal damage in p62 knockout (p62KO) HeLa cells as compared with WT HeLa cells. We utilized a HaloTag-LC3 pulse-chase assay, measuring the formation of a free HaloTag degradation product from the HaloTag-LC3 fusion protein.[55] We treated cells with 1.0 mM LLOMe for 2 h before a 24-h washout period, collecting cell lysates both immediately after the LLOMe treatment period and following 24-h washout. In parallel, we treated cells with 100 nM bafilomycin A1 (BafA1) during the washout period to ensure the free HaloTag resulted from autophagic breakdown of HaloTag-LC3.[56] We observed that WT HeLa cells had significantly increased levels of free HaloTag compared with p62KO HeLa cells (135% increase over p62KO) (Figures S3C and S3D), supporting the hypothesis that p62 is required for autophagy following lysosomal damage.

Next, we utilized a well-established lysophagic flux assay, measuring the percentage of cells retaining endogenous galectin-3 puncta following LLOMe treatment and subsequent washout[30,33]; cells retaining endogenous galectin-3 puncta are scored as deficient in lysophagy. We depleted cells of either p62 (siRNA #1: 95% ± 1.3% knockdown; siRNA #2: 91% ± 3.3% knockdown) or ATG5 (siRNA #1: 85% ± 0.76% knockdown, siRNA #2: 85% ± 0.68% knockdown), a required component of the autophagosome elongation complex[24] (Figures S3A and S3B). Depletion of either p62 or ATG5 significantly decreased lysophagic flux as compared with control siRNA-treated cells (Figures 3F and 3G). The strong inhibition of the engulfment of damaged lysosomes by LC3B-positive membranes and the potent inhibition of lysophagic flux in cells depleted of p62 highlights a key non-redundant role for this adaptor in the selective removal of damaged lysosomes.

P62 oligomerization is critical in lysophagy

Next, we evaluated which domains of p62 are required for lysophagy (Figure 4A). p62 interacts with ubiquitinated cargo via its C-terminal ubiquitin-associated domain (UBA)[57] and with ATG8-family proteins within the developing phagophore via an LC3-interacting region (LIR) motif.[58] Mutating the LIR motif in p62, ^{335}DDDW^{338}, to alanine residues blocks interaction with ATG8-family proteins.[37,59,60] p62 also has an N-terminal Phox and Bem1p (PB1) domain that drives homo-oligomerization.[54,61]

We first tested which domains are critical for p62 translocation to damaged lysosomes, evaluating the recruitment of mCherry-WT p62 (WT), mCherry-p62ΔUBA (ΔUBA), mCherry-p62ΔPB1 (ΔPB1), or mCherry in p62KO cells following damage with 750 μM LLOMe for 2 h (Figure 4B). Both ΔUBA and ΔPB1 displayed reduced localization to damaged lysosomes (Figures 4B, 4C, S4A, and S4B). These findings indicate that the loss of oligomerization prevents the localization of p62 to damaged lysosomes, while the loss of ubiquitin binding reduces recruitment to lysosomes.

We were surprised that p62ΔUBA partially localized to damaged lysosomes, because this construct lacks the well-characterized ubiquitin-binding domain. Thus, we asked whether the localization of ΔUBA depended on expression of another autophagy adaptor. We expressed either WT, ΔUBA, ΔPB1, or a mCherry vector control in pentaKO HeLa. We observed a more complete inhibition of localization of ΔUBA to damaged lysosomes in pentaKO HeLa as compared with the partial loss observed in p62KO cells (Figures 4B, 4C, and S4C-S4F). These results suggest that p62 can cooperatively localize to damaged lysosomes through interactions with another ubiquitin-binding adaptor. NBR1 has a similar domain architecture to p62, including a PB1 domain.[54] Thus, we transiently co-expressed ΔUBA with either EGFP-NBR1 or a GFP vector control. We observed a significant increase in ΔUBA puncta area per cell in the presence of EGFP-NBR1 (Figures S4G-S4J), suggesting that in p62KO cells, p62ΔUBA may localize to damaged lysosomes through an interaction with NBR1.

We next investigated whether loss of p62 at damaged lysosomes diminishes initiation of lysophagy. We transiently expressed FLAG-LAMTOR2 alongside either WT, ΔPB1, ΔUBA, or mCherry in p62KO HeLa cells. Immunostaining for endogenous LC3B indicated a significant increase in LC3B intensity in cells expressing WT-p62 as compared with p62KO cells expressing the mCherry vector control (Figures 4D and 4E). Loss of the UBA domain did not lead to a significant difference in LC3B intensity at LAMTOR2 puncta as compared with WT, likely because of cooperative interactions with NBR1, as described above. In contrast, LC3B intensity was significantly lower in p62KO cells expressing the ΔPB1 construct as compared with cells expressing WT-p62 (Figures 4D, 4E, S3E, and S3F). Together, these data indicate that inhibition of the ability of p62 to self-associate has a potent inhibitory effect on lysophagy.

We performed analogous experiments in HeLa cells following transient p62 knockdown. We observed similar results in which knockdown of p62 and expression of either mCherry alone or p62ΔPB1 failed to rescue LC3B intensity at LAMTOR2-positive lysosomes, as compared

with control cells (Figures S3G-S3J). These results further support an essential role for the PB1 domain of p62 in lysophagy.

We next sought an additional way to test the requirement of the PB1 domain of p62 in lysophagy initiation. In aggrephagy, p62 recruitment facilitates autophagosome formation via recruitment of FIP200, a component of the autophagy initiation complex. FIP200 recruitment results in the local generation of phosphatidylinositol 3-phosphate, which in turn induces recruitment of WIPI2.[37,62] Therefore, we assayed whether p62 is required for Halo-WIPI2b puncta formation following 2 h of 750 μM LLOMe. We observed that p62 knockdown resulted in significantly fewer WIPI2b puncta as compared with control siRNA (Figures 4F and 4G), whereas co-expression of siRNA-resistant WT p62 construct rescued formation of WIPI2b puncta to control levels. In contrast, no rescue was observed on expression of either mCherry vector or the siRNA-resistant ΔPB1 construct (Figures 4F, 4G, S5A, and S5B). Thus, lysophagy requires p62 oligomerization early in the autophagy cascade.

The small heat shock protein HSP27 and p62 dynamically interact in lysophagy

p62 oligomers undergo liquid-liquid phase separation to form p62 condensates.[36,54,61,63] In aggrephagy, these p62 condensates incorporate both aggregated proteins and the autophagy machinery.[64] However, it remains an open question whether p62 condensates have a significant role in organellophagy, the selective autophagy of whole organelles.

We hypothesized that p62 phase separation has a significant role in lysophagy, and proteins that interact with the PB1 domain of p62 may regulate the properties of these condensates. Recently, the small heat shock protein HSP27 (also referred to as HSPB1) has been shown in proximity of damaged lysosomes using APEX2-based proteomics.[33] Importantly, HSP27 interacts with p62 via the PB1 domain.[65] HSP27 incorporates into Fused in sarcoma (FUS) and TAR DNA-binding protein 43 (TDP-43) protein condensates and is crucial for preventing the aggregation of FUS and TDP-43 condensates.[66,67] Therefore, we hypothesized that an interaction between HSP27 and the PB1 domain of p62 might regulate the ability of p62 to form liquid-like condensates on damaged lysosomes.

We first tested whether HSP27 localizes to damaged lysosomes. We transiently co-expressed mCh-LAMTOR2 and EGFP-HSP27 for 24 h before treating HeLa cells with 750 μM LLOMe and simultaneously live-cell imaging. LAMTOR2 puncta formed within ~20 min of lysosomal damage, whereas HSP27 was recruited to LAMTOR2 puncta following ~40 min of lysosomal damage (Figures 5A-5C) (Video S4). Following 2-h treatment with LLOMe, 89% ± 3.2% of LAMTOR2 puncta were co-labeled by EGFP-HSP27, suggesting that the majority of damaged lysosomes recruit HSP27 (Figure 5D). Importantly, the timing of HSP27 localization corresponds to previous reports describing the activation of lysophagy.[20]

We next tested whether endogenous HSP27 responds to lysosomal damage. HSP27 is phosphorylated at serine 15, 78, and 82 in response to oxidative stress and hyperosmotic stress.[68,69] Thus, we assayed whether lysosomal damage induced by LLOMe was sufficient to induce HSP27 phosphorylation. We observed a small, significant decrease in total HSP27 (Figure S6A) and a robust, significant increase in HSP27 phosphorylation following LLOMe

treatment (Figures 5E-5J), suggesting that HSP27 dynamically responds to lysosomal damage.

We then visualized endogenous HSP27 localization following lysosomal damage using immunofluorescence. Endogenous phospho-HSP27 was recruited to lysosomes following LLOMe treatment (Figures 5K-5M) and showed increased co-localization with p62 following LLOMe treatment (Figure 5N). We also evaluated the localization of transiently overexpressed HSP27 in HeLa following lysosomal damage and observed similar increases in HSP27 co-localization with endogenous lysosomal LAMP1 and p62 (Figures S6B-S6E). In i^3Neurons, we observed that transiently expressed EGFP-HSP27 formed puncta following treatment with 1.0 mM LLOMe for 2 h (Figure S6F). Together, these findings demonstrate that HSP27 dynamically responds to lysosomal damage in both HeLa cells and neurons, and that HSP27 is recruited to p62-positive damaged lysosomes.

We next asked whether HSP27 phosphorylation regulates the response of HSP27 to LLOMe by testing whether mutation of S15, S78, and S82 to alanine residues inhibited HSP27 puncta formation following lysosomal damage. EGFP-WT HSP27 and the 3X-phospho-mimetic mutant (EGFP-S15D/S78D/S82D HSP27) responded similarly to lysosomal damage, measuring the number of HSP27 puncta per cell in single z-plane images (Figures S6G-S6J). However, 3x-phospho-dead HSP27 (EGFP-S15A/S78A/S82A HSP27) formed significantly fewer puncta per cell (Figures S6G and S6H), suggesting that HSP27 phosphorylation is necessary for the recruitment of HSP27 to damaged lysosomes.

Next, we asked whether HSP27 and p62 arrive on damaged lysosomes sequentially or simultaneously. To compare the recruitment kinetics of HSP27 and p62, we transiently co-expressed EGFP-HSP27 and mCh-p62 before treating cells with 750 μM LLOMe and live-cell imaging. We observed that 96% ± 1.4% of EGFP-HSP27 was co-localized with mCh-p62 (Figures 5O and 5P) (Video S5). Moreover, we observed that EGFP-HSP27 accumulates on p62 puncta following lysosomal damage (Figure 5Q).

We next tested the requirement for p62 in the recruitment of HSP27 to damaged lysosomes. HSP27 interacts with p62 via the PB1 domain,[65] and loss of the PB1 domain prevented p62 from localizing to damaged lysosomes (Figures 4B and 4C). Similarly, mutagenizing p62 to prevent its oligomerization results in reduced translocation of p62 to *S. typhimurium* in HeLa cells.[60] Alanine substitutions of K7 and D69 in the PB1 domain of p62 are sufficient to prevent p62 oligomerization (Figure 5R).[54,60] Following LLOMe treatment, we observed significantly fewer HSP27 puncta per cell in p62KO HeLa cells expressing either ΔPB1 or K7A/D69A p62 as compared with WT-p62 (Figures 5S and 5T), with no changes to cell area or EGFP-HSP27 fluorescence intensity (Figures 5U and 5V). Therefore, HSP27 requires p62 to translocate to damaged lysosomes.

We asked whether HSP27-p62 interaction is disrupted by K7A/D69A mutations in p62. We immunoprecipitated EGFP-HSP27 and assayed for pull-down of WT-p62, ΔUBA, ΔPB1, K7A/D69A p62, or mCherry alone in p62KO HeLa cells (Figures 5W and S6K). HSP27 immunoprecipitated equivalently across conditions, with no change in binding to HSP90, a known interactor of HSP27, across conditions[70] (Figures S6K-S6M). However, we noted

distinct differences in association of the p62 constructs with HSP27. Co-precipitation with HSP27 was observed from cells expressing WT-p62, ΔUBA, or K7A/D69A p62, but not from cells expressing either p62ΔPB1 or the mCherry vector (Figures 5W and 5X). Taken together, these results demonstrate that HSP27 requires an interaction with p62 to translocate to damaged lysosomes. Moreover, loss of p62 recruitment to damaged lysosomes, as observed in the K7A/D69A p62 mutant construct, is sufficient to diminish HSP27 localization to damaged lysosomes, without disrupting the interaction between p62 and HSP27.

The small heat shock protein HSP27 regulates p62 condensates to promote lysophagy

To test the requirement for HSP27 in lysophagy, we first evaluated co-localization between EGFP-HSP27 and HaloTag-DFCP1 (double FYVE domain-containing protein 1) in live-cell assays. DFCP1 marks PtdIns(3)P-rich extensions of the endoplasmic reticulum (ER) from which autophagosomes originate.[71] We observed striking co-localization between HaloTag-DFCP1 and EGFP-HSP27 beginning at ~50 min of lysosomal damage (Figures 6A and 6B) (Video S6). After 2 h of LLOMe treatment, 94% ± 1.4% of HSP27 puncta co-localized with DFCP1 (Figure 6B). We then evaluated the co-localization between EGFP-HSP27 and mCherry-LC3B (Figure S6N). Using live-cell imaging, we observed that the 85% ± 5.6% of HSP27 puncta co-localized with LC3B after 2 h of LLOMe (Figures S6N and S6O). These results indicate that HSP27 is recruited to sites of lysophagy, co-localizing with DFCP1 and LC3B; further, HSP27 recruitment may precede phagophore formation.

We next tested whether HSP27 is required for lysophagic flux, evaluating the clearance of galectin-3 following lysosomal damage over time.[30,33] We depleted cells of HSP27 (siRNA #1:82% ± 2.9% knockdown; siRNA #2: 83% ± 4.0% knockdown) or ATG5 (siRNA #1: 83% ± 2.9% knockdown; siRNA #2: 86% ± 4.4% knockdown) (Figures S6P and S6Q) and observed that HSP27 or ATG5 depletion decreased lysophagy as compared with control cells, as measured by the fraction of cells retaining galectin-3 over time (Figures 6C and 6D).

We then tested whether HSP27 regulates the initiation of lysophagy at p62-labeled damaged lysosomes. We transiently transfected either control siRNA or HSP27 siRNA for 48 h before treating cells with 750 μM LLOMe for 2 h. We performed immunocytochemistry to evaluate the association of GABARAPs to p62-positive damaged lysosomes. Following LLOMe treatment, we observed a significant decrease in GABARAP area overlapping with and intensity at p62 area in cells depleted of HSP27 as compared with control cells (Figures 6E-6G). However, we observed no significant decrease in p62 association with lysosomes or in LAMP1 area between conditions (Figures S6R and S6S). These results demonstrate that p62 requires HSP27 to promote lysophagy.

The liquidity of selective autophagy cargo regulates the engulfment of the cargo by autophagosomes. Either increased or decreased liquidity of condensates can impair cargo degradation.[72] Therefore, we tested whether loss of HSP27 affects p62 condensates, examining fluorescence recovery after photo-bleaching. If HSP27 maintains the liquidity of p62 condensates, we expected to observe decreased fluorescence recovery over time, indicative of a more gel-like p62 assembly.[73] We transiently transfected HeLa cells with

either control siRNA or HSP27 siRNA (#1) alongside EGFP-p62. After 48 h of expression, we damaged lysosomes with 750 μM LLOMe for 1 h before photo-bleaching EGFP-p62 ring structures and measuring fluorescence recovery (Figure 6H). Depletion of HSP27 resulted in slower fluorescence recovery as compared with control cells (Figures 6H and 6I) (Video S7). Similarly, we quantified the immobile fraction of p62 using the fluorescence recovery assay. The immobile fraction reflects the solid-state p62 or fraction of p62 that did not exchange with the cytosolic p62.[73] We found a significant increase in the immobile fraction of EGFP-p62 following knockdown of HSP27 (Figure 6J). These results demonstrate that HSP27 functions to maintain the liquidity of p62 condensates at damaged lysosomes, affecting the ability of the cell to locally assemble an autophagosome.

ALS-associated mutations in p62 perturb lysophagy

ALS is a fatal neurodegenerative disease targeting the motor neurons of the brain and spinal cord.[74-76] Mutations in p62 have been identified in patients with sporadic and familial ALS.[77,78] Thus, we wondered whether ALS-associated mutations in p62 affect lysophagy. We focused on the well-characterized point mutations in p62 (L341V, P392L, and G425R) (Figure 7A). L341V maps to the LIR motif, residing in the ATG8-binding pocket.[79,80] Importantly, the L341V mutation significantly reduces binding of p62 to ATG8 proteins.[81] P392 is in the UBA domain of p62 but is remote to the ubiquitin binding pocket. P392L results in decreased binding of p62 to polyubiquitin.[82-84] G425 is within the ubiquitin-binding pocket of the UBA domain, and G425R results in complete loss of ubiquitin binding and decrease in aggregate clearance.[83,84]

We first assayed the localization of L341V, P392L, or G425R following lysosomal damage. In HeLa cells depleted of endogenous p62, we rescued with either WT, L341V, P392L, or G425R p62, observing that the L341V, P392L, and G425R mutants each resulted in reduced localization to LAMP1 vesicles as compared with WT-p62 (Figures 7B and 7C). We observed no significant differences in control conditions (Figures S7A and S7B).

Finally, we assayed whether the P392L or G425R mutants affected ATG8 levels at damaged lysosomes. These mutants had the strongest mis-localization effect; thus, we hypothesized that rescue with either P392L or G425R would decrease lysophagy. Consistent with this hypothesis, in HeLa cells depleted of endogenous p62, we observed that P392L or G425R mutants had reduced LC3B intensity as compared with WT-p62 (Figures 7D, 7E, and S7C). Again, we observed no differences in control conditions (Figures S7D and S7E). Therefore, ALS-associated mutations that disrupt the ability of p62 to bind ubiquitin lead to reduced lysophagy.

DISCUSSION

Lysophagy is the primary mechanism by which ruptured lysosomes are degraded. In cell lines, induction of lysosomal damage induces the recruitment of several autophagy adaptors, including TAX1BP1, NDP52, and p62.[18,33] Here, we report the robust recruitment of p62 to damaged lysosomes using different lysosomal injury paradigms in both HeLa cells and neurons. In contrast, we observed limited recruitment of TAX1BP1, and no significant recruitment of NDP52 or OPTN, in i^{3}Neurons. Further, we find that p62

is both necessary and sufficient for lysophagy initiation. Depletion of p62 significantly decreased the accumulation of WIPI2b puncta following lysosomal damage. WIPI2b is required for the expansion of the phagophore.[85] We also find that p62 is required for the turnover of damaged lysosomes, because loss of p62 results in decreased lysophagic flux. Together, these data demonstrate that lysophagy requires p62 recruitment early in the autophagy cascade, likely prior to autophagosome formation. TAX1BP1 is also required for lysophagy,[18] likely recruiting TBK1, an autophagy-promoting kinase. TBK1 has several roles in autophagy, including the promotion of autophagosome maturation.[86] Therefore, we propose a model in which p62 is recruited to damaged lysosomes leading to autophagosome formation, whereas TAX1BP1 recruitment promotes lysophagy via the regulation of autophagosome maturation.

Through domain-mapping experiments, we observed that the PB1 domain of p62 plays a critical role in lysophagy. The PB1 domain of p62 facilitates self-oligomerization, allowing phase condensates of p62 to form, leading us to ask whether p62 condensates are involved in lysophagy. In particular, we focused on the hypothesis that the small heat shock protein HSP27 regulates p62 condensates following lysosomal damage. HSP27 has been shown to incorporate into liquid-phase separated condensates in other contexts, yet a role for HSP27 in regulating the liquidity of p62 condensates had not yet been examined.[66,67] Consistent with our hypothesis, we observed that depletion of HSP27 decreased the liquid-phase properties of p62 recruited to damaged lysosomes. Depletion of HSP27 also inhibited lysophagy initiation and decreased the autophagic turnover of damaged lysosomes. The functional interaction between HSP27 and p62 during lysophagy described here prompts further biophysical investigations, addressing how HSP27 affects the structure and stability of p62 oligomers.

We also observed striking phosphorylation of HSP27 at multiple sites following lysosomal damage. Phosphorylation of HSP27 is critical in lysophagy, because blocking phosphorylation is sufficient to disrupt the recruitment of HSP27 to damaged lysosomes. Phosphorylation of HSP27 has been shown to regulate the incorporation of HSP27 into FUS condensates, preventing FUS aggregation.[66] Therefore, we propose that HSP27 is phosphorylated in order to facilitate incorporation into p62 condensates. Strikingly, in live-imaging experiments, we find that HSP27 recruitment is coincident with the initiation of autophagosome formation. Thus, we suggest that HSP27 is phosphorylated to maintain liquid-like properties of p62 condensates, and that this liquidity is required for autophagosome initiation at damaged lysosomes (Figure 7F). However, this model remains to be tested more fully.

Interestingly, both HSP27 and p62 have been implicated in neurodegenerative disease. Mutations in HSP27 are causative for distal hereditary motor neuropathy and Charcot-Marie Tooth disease type 2F.[87] *In vitro*, disease-causing mutation of HSP27 results in decreased basal and selective autophagy.[65,88] HSP27 is also decreased in motor neurons from ALS patients.[67] Mutations in p62 have been identified in patients with both sporadic and familial cases of ALS.[89] We find that disease-associated mutations in p62 (L341V, P392L, and G425R) decrease p62 localization to damaged lysosomes, and the P392L and G425R mutants of p62 are unable to rescue LC3B intensity at damaged lysosomes, thus indicating

decreased lysophagy. Recent work has shown that several ALS-associated mutations in p62 cause decreased liquidity in p62 condensates.[90] Thus, deficits in p62 localization or decreased liquidity in p62 condensates may be involved in pathophysiology of ALS. Importantly, multisystem proteinopathy, which includes the neurodegenerative aspects of ALS, has been linked previously to lysophagy, because disease-causing mutations in Valosin-containing protein result in defective lysophagy.[30] Therefore, impaired lysophagy could represent a common characteristic in proteinopathies such as ALS.

In summary, our results demonstrate that p62 functions as a lysophagy adaptor. Our results also demonstrate that p62 likely serves as a platform for autophagosome biogenesis in lysophagy. This platform requires precise tuning by HSP27, which maintains the liquidity of p62 condensates and prevents the formation of a more gel-like condensate (Figure 7F). The interaction between p62 and HSP27 may be conserved in other cellular contexts, because both proteins are known to respond to cellular stress conditions.[65,68,69,91] Moreover, both p62 and HSP27 previously have been implicated in ALS.[67,77] Further investigation into the relationship between p62 and HSP27 may uncover mechanisms that can be therapeutically targeted to treat proteinopathies such as ALS, as well as other disorders of lysosomal dysfunction.

Limitations of the study

In our work, we demonstrate a significant role for the selective autophagy adaptor p62 and its interacting partner HSP27 in lysophagy. However, we acknowledge specific limitations in our assays. First, damaged lysosomes can undergo direct ATG8 conjugation; thus, the observable shifts in LC3B/GABARAP intensities following manipulation of p62 or HSP27 are restricted. However, in combination with lysophagic flux assays and WIPI2b puncta formation assays, we are able to discern a clear role for both HSP27 and p62 in lysophagy. Second, lysophagy flux assays are inherently challenging to design and interpret, because damaged lysosomes can undergo reformation and re-acidification concomitant with lysophagy. Therefore, it is necessary to use multiple complementary assays to measure lysophagy in cellular experiments.

STAR★METHODS

RESOURCE AVAILABILITY

Lead contact—Further information and requests for resources and reagents should be directed to and will be fulfilled by the lead contact, Erika L.F. Holzbaur (holzbaur@pennmedicine.upenn.edu).

Materials availability—All unique/stable reagents generated in this study are available from the lead contact with a completed Materials Transfer Agreement.

Data and code availability

- This paper does not report original code.
- All data reported in this paper will be shared by the lead contact upon request.

- Any additional information required to reanalyze the data reported in this paper is available from the lead contact upon request.

EXPERIMENTAL MODEL AND SUBJECT DETAILS

HeLa-M cells (referred to here as HeLa) (A. Peden, Cambridge Institute for Medical Research) were authenticated by STR profiling. HEK293 were authenticated by STR profiling. WT HeLa, p62KO HeLa, and pentaKO HeLa were gifts from Richard Youle (National Institutes of Health). All HeLa and HEK cells were cultured in Dulbecco's Modified Eagle's Medium (Corning - MT10-013-CV or Gibco - 11965084), which was supplemented with 10% Fetal Bovine Serum and 1% GlutaMax (Thermo - 35050061). Cells were cultured in a 5% CO_2 incubator at 37 C. Cells were tested for mycoplasma contamination routinely, using MycoAlert detection kit (Lonza, LT07).

Embryonic mouse neurons were dissected at E15.5, and were plated onto 0.5 mg/mL poly-L-lysine coated 6-well plates for lysate collections. Primary rat hippocampal neurons were received from the Neurons R Us Culture Service Center at the University of Pennsylvania. Prior to receiving cells, 35-mm glass-bottom dishes (MatTek) were coated with 0.5 mg/mL poly-L-lysine (Sigma) overnight at 37 C. Primary neurons were plated at 220,000 cells per dish into attachment media (MEM supplemented with 10% horse serum, 33mM D-glucose, and 1mM sodium pyruvate). Following attachment (4-6hrs), attachment media was removed and replaced with maintenance media (Neurobasal [Gibco] supplemented with 33mM D-glucose [Sigma], 2mM GlutaMax [Gibco], Penicilin (100units/mL)/Streptomycin (100µg/mL) [Giibco], and 2% B27 [Gibco]). On the following day, 5µM AraC [Sigma] was added to the cultures to prevent proliferation of non-neuronal cells. Neurons were cultured with 5% CO_2at 37 C for 7–10 days prior to transfection.

Human LAMP1-eGFP i^{3}Neuron iPSCs were generated previously.[48] iPSCs were cultured in Essential 8 medium [Thermo Fisher] and plated onto Matrigel coated dishes. An established protocol was used for neuronal differentiation into i^{3}Neurons.[49] Following differentiation, i^{3}Neurons were cryo-preserved in i^{3}Neuron media (BrainPhys Neuronal Medium supplemented [StemCell] with 2% B27 [Gibco], 10 ng/mL BDNF [PeproTech], 10 ng/mL NT-3 [PeproTech], and 1 µg/mL Laminin [Corning]) with 10% DMSO added. Prior to culturing i^{3}Neurons, 35-mm glass-bottom dishes [MatTek] were coated with poly-L-ornithine overnight at 37 C i^{3}Neurons were cultured for 21–22 days in 5% CO_2 at 37 C and were fed every 3–4 days with fresh i^{3}Neuron media culture media.

METHOD DETAILS

Antibodies—The following primary antibodies were used: rabbit polyclonal anti-LAMP1 (Abcam, ab24170, Lot: GR3409154, WB: 1:1000, IF: 1:500); sheep polyclonal anti-LAMP1/CD107a (R&D Systems, AF4800, Lot: CAYN022012A, CAYN022107B, CAYN0221081, IF: 1:40); sheep polyclonal anti-LAMP1/CD107a Alex Flour 488-conjugated (R&D Systems, IC7985G, Lot: ADNG0420101, ADNG0420041, IF: 1:40); mouse monoclonal anti-p62 (Abcam, ab56416, Lot: GR3367558, GR3397093, IF: 1:500); guinea pig polyclonal anti-p62 (American Research Products, 03-GP62-C, Lot: 703,241-03, WB: 1:3000); rabbit polyclonal anti-FIP200 (Proteintech, 17250-1-AP, Lot: 0,050,110, WB:

1:1000); rabbit monoclonal anti-TAX1BP1 (Abcam, ab176572, Lot: GR137934, IF: 1:200, WB: 1:1000), rabbit monoclonal anti-GABARAP (E1J4E) (Cell Signaling, 13,733, Lot: 3, WB: 1:1000); rabbit monoclonal anti-GABARAP + GABARAPL1+GABARAPL2 (Abcam, ab109364, Lot: GR3232141, IF: 1:100); rabbit polyclonal anti-LC3b (Novus Biologicals, NB100-2220, Lot: DP-1, WB: 1:1000); rabbit polyclonal anti-LC3b (Abcam, ab48394, Lot: GR3401900, GR3374546, GR3339674, IF: 1:200); rabbit polyclonal anti-NDP52 (Abcam, ab68588, Lot: GR197350; IF: 1:200); rabbit polyclonal anti-OPTN (Abcam, ab23666, Lot: GR271296, IF: 1:200); rabbit monoclonal anti-Tau (Abcam, ab8763, Lot: 158781, IF: 1:200); mouse monoclonal anti-Tau (Sigma, MAB3420, Lot: 2876166, IF: 1:1000); mouse monoclonal anti-Galectin-3 (Santa Cruz Biotech, sc-32790, Lot: G1620, IF: 1:50); rabbit polyclonal anti-Galectin-8 (Abcam, ab42879, Lot: abGR3277211, WB: 1:1000); mouse monoclonal anti-Hsp27 (Santa Cruz Biotech, sc-13132, Lot: I0821, WB: 1:200); rabbit monoclonal anti-pSer15 Hsp27 (Sigma, SAB4300134, Lot: 871511164, WB: 1:500); rabbit anti-pSer78 Hsp27 (Cell Signaling, 2405, Lot: 4, WB: 1:1000); rabbit anti-pSer82 Hsp27 II (Cell Signaling, 2406, Lot: 3, WB: 1:1000); rabbit monoclonal anti-HSP90 (C45G5) (Cell Signaling, 4877T, Lot: 5, WB: 1:1000); chicken polyclonal anti-mCherry (Abcam, ab205402, Lot: GR3176028, GR3368071, GR3424850, WB: 1:1000, IF: 1:200); chicken polyclonal anti-GFP (Aves Lab, GFP-1020, Lot: GFP3717982, WB: 1:1000; IF: 1:1000); mouse monoclonal anti-GFP (Abcam, ab1218, Lot: GR3392723, IF: 1:200, IP: 1.25μg/condition); mouse monoclonal anti-HA-Tag (16B12) Alexa flour-594 (Invitrogen, A21288, Lot: 2,218,838, IF: 1:100); mouse monoclonal anti-FLAG M2 (Sigma, F3165, Lot: SLBG5673V, SLCF4933,SLCJ4124, SLCK5688, IF: 1:200); rabbit polyclonal anti-HaloTag (Promega, G9281, Lot: 0,000,514,949, WB: 1:1000); rabbit anti-α/β-tubulin (Cell Signaling, 2148, Lot:8, WB: 1:1000); mouse anti-GAPDH (Abcam, ab9484, Lot: GR3299150-9, WB: 1:1000); rabbit anti-LAMTOR2/p14 (Abcam, ab183514, Lot: GR153673-4, WB: 1:1000)

The following secondary antibodies were used for immunofluorescence: Alexa Fluor 488 goat anti-rabbit IgG (H + L) (Invitrogen, A11034, Lot: 2256692); Alexa Fluor 594 goat anti-rabbit IgG (H + L) (Invitrogen, A11037, Lot: 2307302, 1915919); Alexa Fluor 647 goat anti-rabbit IgG (H + L) (Invitrogen, A31573, Lot: 2359136); Alexa Fluor 488 goat anti-chicken IgG (H + L) (Invitrogen, A11039, 2079383); Alexa Fluor 555 goat anti-chicken IgG (H + L) (Invitrogen, A21437, Lot: 1719681); Alexa Fluor 594 goat anti-mouse IgG (H + L) (Invitrogen, A11032, Lot: 2129448); goat anti-mouse IgG (H + L) Alexa Fluor Plus 647 (Invitrogen, A32728, Lot: WK331591, 1826679); Alexa Fluor 594 donkey anti-sheep IgG (H + L) (Invitrogen, A11016, Lot: 536,045); GFP-Booster ATTO 488 (Chromotek, GBA488-100, Lot: 90401001AT1-04). All secondary antibodies were used at a dilution of 1:1000 for immunofluorescence.

The following secondary antibodies were used for Western blot experiments: IRDye 680RD Donkey anti-Guinea Pig (Li-COR, 926-68077, Lot: C70425-05); IRDye 680RD Donkey anti-Chicken (Li-COR, 926-68075, Lot: C70201-50); IRDye 800CW Donkey anti-Mouse (Li-COR, 926-32212, Lot: D10414-15); Alexa Fluor 680 AffiniPure Goat anti-Mouse IgG light chain (Jackson Immuno, 115-625-174, Lot: 131,312); IRDye 680RD Donkey anti-Rabbit (Li-COR, 926-68073, Lot: 91,204-03, D11207-05); IRDye 800CW Donkey anti-Rabbit (Li-COR, 926-32213, Lot: D00304-05).

Plasmids—ptf-Galectin-3 was a gift from Tamotsu Yoshimori (Addgene plasmid # 64149).[28] GFP-Galectin-3 was subcloned from ptf-Galectin-3 (Addgene: 64,149). pMXs-puro eGFP-p62 was a gift from Noboru Mizushima (Addgene plasmid # 38 2 77).[97] HaloTag-p62 was subcloned from eGFP-p62 (Addgene plasmid # 38277) into pHTN Halo-Tag vector (Promega). mCherry-WT-p62, mCherry-p62ΔPB1, mCherry-p62ΔUBA, mCherry-p62 K7A/D69A, and pmCherry-C1 [Clontech] were gifts from S. Martens (Max Perutz Labs, University of Vienna).[60] ALS-associated mutations in p62 (L341V, P392L, and G425R) were generated via site-directed mutagenesis of mCherry-WT-p62. eGFP-hWT-p62 was subcloned from mCherry-WT-p62 into eGFP-N1. pLJC5-Tmem192-3xHA was a gift from David Sabatini (Addgene plasmid # 102930).[41] pRK5-FLAG-LAMTOR2 was a gift from David Sabatini (Addgene plasmid # 42330).[95] mCherry-LAMTOR2 was subcloned from FLAG-LAMTOR2 into pmCherry-C1 [ClonTech]. HaloTag-TAX1BP1 was purchased form Promega. eGFP-TAX1BP1 was generated by subcloning from HaloTag-TAX1BP1.[93] eGFP-NBR1 was a gift from Peter Kim (The Hospital for Sick Children, University of Toronto).[99] pAc-GFP-C1 vector was purchased from Clontech. LAMP1-KillerRed was subcloned from LAMP1-RFP. LAMP1-RFP was a gift from Walther Mothes (Addgene plasmid # 1817).[100] LAMP1-KillerRed was subcloned into KillerRed-dMito [Evrogen]. LAMP1-HaloTag was subcloned from LAMP1-RFP into pHTC vector. HaloTag-WIPI2b was subcloned from GFP-WIPI2b.[85,94] Halo-DFCP1 was subcloned from GFP-DFCP1.[94] pMXs-puro GFP-DFCP1 was a gift from Noboru Mizushima (Addgene plasmid # 38269).[101] mCherry-LC3B was subcloned from eGFP-LC3B, which was a gift from Tamotsu Yoshimori (Addgene plasmid # 21073).[102] mCherry-LC3B was subcloned into pmCherry-C1 [Clontech]. HaloTag-LC3B was subcloned from eGFP-LC3B into pHTN-HaloTag. PGK-LAMP1-mNeon was a gift from M. Ward (NIH). LAMP2-BFP was subcloned from eGFP-N1-LAMP2, which was a gift from E. Chapman (UW Madison). pEGFP-HSP27 (WT) was a gift from Andrea Doseff (Addgene plasmid # 174 44).[92] pEGFP-3XSD-HSP27 was subcloned from pFLAG-CMV2-Hsp27-S15D/S78D/S82D, a gift from Ugo Moens (Addgene plasmid # 85188), into pEGFP-HSP27 (WT). pEGFP-3XSA-HSP27 was subcloned from pFLAG-CMV2-Hsp27-S15A/S78A/S82A, a gift from Ugo Moens (Addgene plasmid # 84997), into pEGFP-HSP27 (WT). pCMV-VSV-G was a gift from Bob Weinberg (Addgene plasmid # 8454).[103] psPAX2 was a gift from Didier Trono (Addgene plasmid # 12260).

Transfection—For fixed and live-cell experiments without siRNA, HeLa cells, p62KO HeLa cells, and pentaKO cells were transfected with 0.3-1.5μg of DNA using FuGene 6 [Promega] and incubated for 24hrs. However, HeLa cells transfected with LAMP1-KillerRed were incubated for 48hrs.

In knockdown experiments, HeLa cells were transfected with 40μM siRNA using Lipofectamine RNAiMax and incubated for 48hrs. To knockdown p62, ON-TARGETplus p62 siRNA (J-010230-05) (#1) or ON-TARGETplus p62 siRNA (J-010230-07) (#2) was used on HeLa cells (Target sequence #1: ‘GAACAGAUGGUCGGAUA’, Horizon Discovery; Target sequence #2: ‘CCACAGGGCUGAAGGAAGC’, Horizon Discovery). To knockdown ATG5, ON-TARGETplus ATG5 siRNA (J-004374-09) (#1) or ON-TARGETplus ATG5 pool siRNA(L-004374-00) (#2) was used on HeLa cells

(Target sequence #1: 'UGACAGAUUUGACCAGUUU,' Horizon Discovery; Target sequences #2: 1: 'GGCAUUAUCCAAUUGGUUU', 2: 'GCAGAACCAUACUAUUUGC', 3: UGACAGAUUUGACCAGUUU', 4: 'ACAAGAUGUGCUUCGAGA', Horizon Discovery). To knockdown HSP27, ON-TARGETplus HSPB1 pool siRNA (L-005269-00) (#1) or ON-TARGETplus HSPB1 siRNA (J-005269-06) (#2) was used on HeLa cells (Target sequences #1:1: 'CAAGUUUCCUCCUCCCUGU,' 2: 'GAGACUGCCGCCAAGUAAA,' 3: 'GGUGCUUCACGCGGAAAUA,' 4: 'CCACGCAGUCCAACGAGAU,' Horizon Discovery; Target sequence #2: 'CAAGUUUCCUCCUCCCUGU,' Horizon Discovery). In knockdown and rescue experiments, HeLa cells were transfected with 40μM siRNA alongside 0.5-1.0μg total DNA using Lipofectamine 2000 and incubated for 48hrs.

Rat hippocampal neurons were transfected following 8-11 days *in vitro*. Neurons were transfected with 0.5-1.0μg of DNA using Lipofectamine 2000. Neurons were incubated with DNA:lipid complexes for 45 min prior to replacement with full conditioned media. Neurons were fixed for immunofluorescence 24hrs later. However, rat hippocampal neurons transfected with LAMP1-KillerRed were incubated for 48hrs prior to live-cell imaging.

LLOMe-induced lysosomal damage—L-Leucyl-L-Leucine methyl ester monohydrochloride (Cayman) was dissolved in 100% ethanol. In fixed cell experiments, HeLa, p62KO, pentaKO were treated with 250μM or 750μM LLOMe for 2hrs prior to fixation. We preferentially used 750μM LLOMe in our HeLa cell experiments, as we measured a smaller standard deviation in p62 recruitment to damaged lysosomes (Figures 1G and 1H). However, in flux assays and lysosomal immunoprecipitations, 1.0mM LLOMe was used to re-capitulate previous experimental paradigms.[18,30] In live cell experiments, HeLa cells were removed from culture media and replaced with HeLa imaging media (Leibovitz's L-15 Medium (Gibco) supplemented with 10% FBS and 1% GlutaMax). Subsequently, 750μM LLOMe was added to HeLa imaging media. For immunofluorescence experiments, rat hippocampal neurons and i^{3}Neurons were treated with 1.0mM LLOMe for 2hrs prior to fixation.

Stable cell line generation—Stable cell lines were generated using lentivirus transduction and subsequent single-cell isolation. In brief, 700,000 HEK293 cells were seeded in a 6-cm dish. The following day, HEK293 cells were transfected with 1μg (LAMP1-mNeonGreen) or 3μg (TMEM192-3xHA) along with packaging plasmids (psPAX2 and VSV-G) using Fugene 6 [Promega]. HEK293 cells were incubated for either 24hr (LAMP1-mNeonGreen) or 36hr (TMEM192-3xHA). Following this, the media was replaced with complete culture media supplemented with Viral Boost Reagent [ALSTEM]. After 24 h, the conditioned media was collected for HeLa transduction and passed through a 45 μm filter.

HeLa were seeded at 50,000 cells in a 6-cm dish on the day before transduction. HeLa media was removed and replaced with virus for 24hrs. Following the transduction, cells were grown until 70% confluency and then single cells were isolated and plated onto a 96-well plate. To isolate single cells, cells were diluted to a final concentration of 5 cells/mL, using an established protocol [Addgene]. Clones were selected by expression level of construct of interest.

Immunoprecipitation—Lysosomal immunoprecipitation experiments were performed following an established protocol.[41] In brief, HeLa TMEM192-3xHA were seeded at 4 million cells/15-cm dish. Approximately 48hr later when cells reach 80% confluence, cells were treated with 1.0mM LLOMe for 1hr or were untreated. Cells were scraped into cold KPBS buffer (1x PBS (50mM $NaPO_4$, 150mM NaCl, pH = 7.4) supplemented with 136mM KCl, 10mM KH_2PO_4, 50mM sucrose, 1mM phenylmethanesulfonyl Fluoride, 20μg/mL TAME, 20μg/mL Leupeptin, 2 μg/mL Pepstatin-A). In the absence of sucrose, LLOMe-treated lysosomes had consistently decreased yields. Cells were spun down and resuspended into 950uL from which 50μL was stored on ice as whole cell fraction. The remainder of the cell suspension was homogenized using 2mL glass homogenizer. Following this, the homogenized lysate is spun down, collecting the resultant supernatant as lysate fraction. Protein concentration of lysate was quantified using a Bradford Concentration Assay (BCA), and then protein concentration was normalized across conditions. Following normalization, 100μL of anti-HA magnetic beads were added to the remainder of the sample. Following incubation, magnetic beads were washed with KPBS buffer containing 300mM NaCl prior to elution. Magnetic beads were eluted into 80μL SDS sample buffer.

eGFP-HSP27 immunoprecipitations were performed in p62KO HeLa cells 24hrs following transient transfection using Fugene 6 (Promega). HeLa cells were treated with 750μM LLOMe for 2hrs prior to immunoprecipitation. Cells were collected into and incubated in lysis buffer (ddH_20 supplemented with 20mM Tris-HCl, 137mM NaCl, 2mM EDTA, 1% NP-40, 5% glycerol, 1mM phenylmethanesulfonyl fluoride, 20μg/mL TAME, 20μg/mL leupeptin, 2 μg/mL pepstatin-A). Following 15min of lysis, lysates were spun, and the supernatant was collected as the lysate fraction. 600μL of lysate was added to Protein G DynaBeads, which had been incubated with 1.25μg Mouse anti-GFP (Abcam, ab1218) for 30 min at 4 C. The magnetic beads were then washed with TBS supplemented with 0.05% Tween 20 (0.05% TBS-T) prior to the addition of lysate. A small fraction of lysate was stored on ice for lysate fraction. Dynabeads were incubated in lysate for 1 h at 4 C, and then were washed with 0.05% TBS-T prior to elution. Magnetic beads were eluted into 60μL SDS sample buffer.

Western blotting—To assay expression levels of proteins in HeLa, i^3Neurons, and mouse cortical neurons, cells were washed 2x with ice-cold PBS prior to lysis with RIPA buffer (50mM Tris-HCl, 150mM NaCl, 0.1% Triton X-100, 0.5% sodium deoxycholate, 0.1% SDS, 2x Halt Protease and Phosphatase inhibitor). Cells were snap frozen in liquid nitrogen prior to incubation in RIPA buffer for 30 min at 4 C. Samples were then centrifuged, and the supernatant was collected as the lysate fraction. A BCA was performed on the collected lysate, and samples were denatured in sample buffer containing SDS at 95 C.

For immunoprecipitation experiments and protein expression experiments, samples were resolved using SDS-PAGE gels. Following electrophoresis, proteins were transferred to Immobilon-FL PVDF membranes [Millipore]. The membrane was dried for 1hr prior to rehydration in methanol. The membranes were then stained for total protein levels, using Li-COR Revert Total Protein stain. The membranes were imaged using an Odyssey CLx Infrared Imaging System (Li-COR). Following imaging, membranes were destained with 0.1M NaOH supplemented with 30% Methanol.

Membranes were then blocked in either TrueBlack WB Blocking Buffer (Biotium) or EveryBlot Blocking Buffer (Bio-Rad). When using TrueBlackWB Blocking Buffer, membranes were blocked for 1 h and were incubated with primary antibodies diluted in TrueBlack WB Antibody Diluent (Biotium) supplemented with 0.2% Tween 20 (Bio-Rad) at 4 C overnight. Alternatively, when membranes were blocked with EveryBlot Blocking Buffer, membranes were blocked for 5-10 min and were incubated with primary antibodies diluted in EveryBlot Blocking Buffer overnight at 4 C. After 12-16 h incubation, membranes were washed 3x with 1xTBS (50mM Tris-HCl, 274mM NaCl, 9mM KCl) supplemented with 0.1% Tween 20 (TBS-T). Membranes were then incubated in secondary antibody, which were diluted in either TrueBlack WB Blocking Buffer supplemented with 0.01% SDS or EveryBlot Blocking Buffer supplemented with 0.02% SDS. Membranes were incubated for 1hr and then were washed 3x with TBS-T. Membranes were then imaged, and band intensities were measured in the Li-COR Image Studio application.

Fixation and permeabilization conditions—A variety of fixation methods were used, depending on antibodies and cell types used and following optimization. In experiments assaying LC3B intensity in HeLa, pentaKO, or p62KO cells, cells were fixed using Bouin's Solution supplemented with 8% sucrose. Bouin's solution was added in a 1:1 ratio with cell media, and cells were incubated for 30 min at room temperature. Cells were washed with PBS prior to permeabilization with ice-cold methanol. In experiments assaying the effect of ALS-associated mutants on LC3B intensity in HeLa cells, cells were fixed in ice-cold methanol.

In experiments assaying WIPI2b-puncta number, cells were fixed with 4% paraformaldehyde supplemented with 4% sucrose (4% PFA/4% sucrose). Cells were incubated with Janelia Fluor 646-Halo ligand [Promega] for 1.5 h in blocking solution (5% goat serum and 1% BSA in PBS).

In experiments assaying co-localization of LAMP1 with adaptors, with GABARAPs, or with eGFP-HSP27 in i^3Neurons or in HeLa cells, cells were fixed with 4% PFA/4% sucrose. Permeabilization was performed with ice-cold methanol. p62 localization experiments in p62KO and pentaKO cells as well as in hippocampal neurons were fixed with 4% PFA/4% sucrose. In the HeLa cells permeabilization was performed with ice-cold methanol. The hippocampal neurons were directly mounted in ProLong Gold anti-fade mountant (ThermoFisher). Similarly, in eGFP-HSP27 puncta formation assays in i^3Neurons or p62KO cells, cells were fixed with 4% PFA/4% sucrose before mounting in ProLong Gold anti-fade mountant.

Immunostaining—Following permeabilization, cells were blocked in blocking solution (5% goat serum and 1% BSA in PBS) for 90 min. Samples were then incubated with primary antibodies overnight at 4 C. Primary antibodies were diluted into blocking solution. After 14–16 h of incubation, cells were washed with PBS and then incubated in secondary antibodies. Secondary antibodies were also diluted into blocking solution. Following secondary antibody incubations, samples were washed with PBS. Frequently, samples were treated with a nuclear counterstain [Hoechst 33,342, Invitrogen] for 10 min. Coverslips were mounted in ProLong Gold [Life Technologies].

Images were acquired using a PerkinElmer UltraView Vox spinning disk confocal on a Nikon Eclipse Ti Microscope. Fixed cell experiments were performed on an Apochromat 100x 1.49NA oil-immersion objective, and live-cell experiments were performed on a Plan Aprochromat Lambda 60× 1.40NA oil-immersion objective. Z-stacks were collected at 200nm step-size. Experiments were imaged on either a Hamamatsu EMCCD C9100-50 camera or a Hamamatsu CMOS ORCA-Fusion (C11440-20UP). The EMCCD camera was used with Volocity Software [Quorom Technologies/PerkinElmer]. The CMOS camera was used with VisiView (Visitron).

Flux assays—To assay lysophagy flux via Halo-LC3 degradation, we utilized an established protocol.[55] In brief, HeLa cells were transfected with 0.6ug of Halo-LC3 24hr in advance. Cells were labeled with 100nM Halo-TMR for 20min before rinses with warm complete media. We damaged lysosomes for 2 h using 1.0mM LLOMe, as this concentration is frequently utilized in lysophagy flux assays.[18,30] Lysates were collected immediately following the 2hr LLOMe treatment, or cells were washed with complete media twice prior to a 24hr washout of LLOMe. As a negative control, cells were treated with 100nM bafilomycin A1 during the washout period, preventing lysosomal re-acidification.

To assay lysophagic flux via clearance of endogenous galectin-3, we utilized an established protocol.[30] In brief, HeLa cells were transiently transfected with siRNAs 48hrs prior to the experiment. Following 48hr of siRNA siRNA expression, we treated cells with 1mM LLOMe for 2 h. Cells were fixed immediately post-LLOMe treatment, or cells were washed with complete media twice prior to a 15hr washout of LLOMe. As a negative control, we transfected cells with ATG5 siRNA in parallel to block autophagosome formation.

Live-cell imaging—For live-cell imaging of HeLa cells, the culture media was replaced with Leibovitz's L-15 media (Gibco, 11,415,064). The media was supplemented with 1% Glutamax and 10% fetal bovine serum. Cells were then moved onto the microscope stage, which is surrounded by a 37°C imaging chamber. The samples were given several minutes to equilibrate before imaging. When using LLOMe, a single frame was captured prior to lysosomal damage treatment. LLOMe was then added directly to the imaging dish, and then cells were imaged for 1 or 2hrs. To avoid photo toxicity and photo-bleaching, cells were imaged a low frame rate (ranging from one frame every minute to one frame every 10 min), depending on the experiment.

In KillerRed experiments, both HeLa and rat hippocampal neurons underwent 7 photo-bleaching cycles with 9ms per pixel. Cells were imaged for either 45min or 1hr post-initial FRAP cycle. In eGFP-p62 fluorescence recovery after photo bleaching experiments, HeLa cells underwent one photo-bleaching cycle with 12ms per pixel. Cells were imaged for 20 min following the photo-bleach.

In experiments using live-cell imaging of rat hippocampal neurons, culture media was removed and replaced with Hibernate E medium, which was supplemented with 2% B27 and 33mM D-glucose.

QUANTIFICATION AND STATISTICAL ANALYSIS

Statistics—Statistical tests were performed in Graphpad prism v9. Experimental data was first tested for normality prior to statistical testing. When appropriate, we performed statistical tests only on averages per independent replicates (N). When using averages per replicate, we graphically represented the data as superplots,[104] plotting all data points (n) included to openly report the spread of data. When the data required normalization to a control condition, we performed statistical tests on all data points included in each independent replicate. All data included is represented as mean and the standard error of the mean, thus error bars in graphs reflect standard error of the mean.

Immunofluorescence quantifications—To measure LC3B/GABARAPs intensity at either Flag-LAMTOR2, mCherry-LAMTOR2, or α-p62 puncta, max projections of each channel in each image were made. Individual cells were selected from these max projections. Cells were selected if they were completely in the frame of the image, were equivalently transfected, were in interphase, and were not blebbing or going through apoptosis. LAMTOR2 area was thresholded and binarized using Otsu thresholding in ImageJ.[105] p62 area was thresholded and binarized using Ilastik segmentation, a machine-learning based approach to image segmentation. The binarized images were used to generate regions of interest, and then LC3B fluorescence intensity was measured within these regions of interest.

To quantify area within the cell occupied by an individual protein, we generated max projections of each channel in every image. Individual cells were selected from these max projections, using similar parameters as listed above. We then segmented the area of these proteins using Ilastik, a machine-learning based approach to image segmentation.[98] The percentage overlap between different proteins was measured using the image calculator function in ImageJ.

Quantification of live-cell data—To quantify fluorescence intensity of eGFP-p62 or LAMP1-KillerRed in KillerRed experiments, we identified regions encapsulating the photo-bleached area or regions outside the photo-bleached area, and measured the intensity at each frame over time using Fiji/ImageJ.

To quantify the fluorescence intensity of mCherry-p62 puncta co-localizing with eGFP-HSP27, we identified mCherry-p62 puncta that remained in frame (z section) for an hour. We then measured the intensity of both channels at every frame for an hour, starting at the frame before HSP27 appeared. We measure intensities over time using Fiji/ImageJ.

To quantify the fluorescence recovery of eGFP-p62 after photo-bleaching, we identified eGFP-p62 puncta that co-localized with LAMP1-RFP prior to photo-bleaching and after treatment with 750μM LLOMe for 1hr. eGFP-p62 was photo-bleached according to the parameters listed in the prior section, and puncta were only included if they retained some of the eGFP-p62 signal in order to track the puncta over time. Fluorescence intensity was measured using Fiji/ImageJ. Additionally, we quantified the immobile fraction of eGFP-p62. The immobile fraction is an established metric of liquid-phase behaviors.[73,106] This fraction is calculated by subtracting the final intensity measurement from the initial fluorescence

intensity measurement. This fraction reflects the relative amount of eGFP-p62 that did not photo-recover.

Supplementary Material

Refer to Web version on PubMed Central for supplementary material.

ACKNOWLEDGMENTS

We thank Mariko Tokito and Andrea Stavoe for technical assistance, and we thank Adam Fenton, Alex Boecker, Sierra Palumbos, and Juliet Goldsmith for insight and discussion. This work was supported by National Institutes of Health grants T32 GM007229 (to E.R.G.), F31 NS125954 (to E.R.G.), and R01 NS060698 (to E.L.F.H.).

INCLUSION AND DIVERSITY

We support inclusive, diverse, and equitable conduct of research.

REFERENCES

1. Appelqvist H, Wäster P, Kågedal K, and Øllinger K (2013). The lysosome: from waste bag to potential therapeutic target. J. Mol. Cell Biol 5, 214–226. 10.1093/jmcb/mjt022. [PubMed: 23918283]
2. Aits S, and Jäättelä M (2013). Lysosomal cell death at a glance. J. Cell Sci 126, 1905–1912. 10.1242/jcs.091181. [PubMed: 23720375]
3. De Duve C (1983). Lysosomes revisited. Eur. J. Biochem 137, 391–397. 10.1111/j.1432-1033.1983.tb07841.x. [PubMed: 6319122]
4. Gabandé-Rodríguez E, Pérez-Cañamás A, Soto-Huelin B, Mitroi DN, Sánchez-Redondo S, Martínez-Sáez E, Venero C, Peinado H, and Ledesma MD (2019). Lipid-induced lysosomal damage after demyelination corrupts microglia protective function in lysosomal storage disorders. EMBO J. 38, e99553. 10.15252/embj.201899553. [PubMed: 30530526]
5. Repnik U, Hafner Česen M, and Turk B (2014). Lysosomal membrane permeabilization in cell death: concepts and challenges. Mitochondrion 19, 49–57. 10.1016/j.mito.2014.06.006. [PubMed: 24984038]
6. Song L, Pei L, Yao S, Wu Y, and Shang Y (2017). NLRP3 inflammasome in neurological diseases, from functions to therapies. Front. Cell. Neurosci 11, 63. 10.3389/fncel.2017.00063. [PubMed: 28337127]
7. Malik BR, Maddison DC, Smith GA, and Peters OM (2019). Autophagic and endo-lysosomal dysfunction in neurodegenerative disease. Mol. Brain 12, 100. 10.1186/s13041-019-0504-x. [PubMed: 31783880]
8. Monaco A, and Fraldi A (2020). Protein aggregation and dysfunction of autophagy-lysosomal pathway: a vicious cycle in lysosomal storage diseases. Front. Mol. Neurosci 13, 37. 10.3389/fnmol.2020.00037. [PubMed: 32218723]
9. Nixon RA (2013). The role of autophagy in neurodegenerative disease. Nat. Med 19, 983–997. 10.1038/nm.3232. [PubMed: 23921753]
10. Usenovic M, and Krainc D (2012). Lysosomal dysfunction in neurodegeneration: the role of ATP13A2/PARK9. Autophagy 8, 987–988. 10.4161/auto.20256. [PubMed: 22561922]
11. Wallings RL, Humble SW, Ward ME, and Wade-Martins R (2019). Lysosomal dysfunction at the centre of Parkinson's disease and frontotemporal dementia/amyotrophic lateral sclerosis. Trends Neurosci. 42, 899–912. 10.1016/j.tins.2019.10.002. [PubMed: 31704179]
12. Root J, Merino P, Nuckols A, Johnson M, and Kukar T (2021). Lysosome dysfunction as a cause of neurodegenerative diseases: lessons from frontotemporal dementia and amyotrophic lateral sclerosis. Neurobiol. Dis 154, 105360. 10.1016/j.nbd.2021.105360. [PubMed: 33812000]

13. Udayar V, Chen Y, Sidransky E, and Jagasia R (2022). Lysosomal dysfunction in neurodegeneration: emerging concepts and methods. Trends Neurosci. 45, 184–199. 10.1016/j.tins.2021.12.004. [PubMed: 35034773]

14. Freeman D, Cedillos R, Choyke S, Lukic Z, McGuire K, Marvin S, Burrage AM, Sudholt S, Rana A, O'Connor C, et al. (2013). Alpha-Synuclein induces lysosomal rupture and cathepsin dependent reactive oxygen species following endocytosis. PLoS One 8, e62143. 10.1371/journal.pone.0062143. [PubMed: 23634225]

15. Gabandé-Rodríguez E, Boya P, Labrador V, Dotti CG, and Ledesma MD (2014). High sphingomyelin levels induce lysosomal damage and autophagy dysfunction in Niemann Pick disease type A. Cell Death Differ. 21, 864–875. 10.1038/cdd.2014.4. [PubMed: 24488099]

16. Jiang P, Gan M, Yen S-H, McLean PJ, and Dickson DW (2017). Impaired endo-lysosomal membrane integrity accelerates the seeding progression of α-synuclein aggregates. Sci. Rep 7, 7690. 10.1038/s41598-017-08149-w. [PubMed: 28794446]

17. Vitner EB, Dekel H, Zigdon H, Shachar T, Farfel-Becker T, Eilam R, Karlsson S, and Futerman AH (2010). Altered expression and distribution of cathepsins in neuronopathic forms of Gaucher disease and in other sphingolipidoses. Hum. Mol. Genet 19, 3583–3590. 10.1093/hmg/ddq273. [PubMed: 20616152]

18. Eapen VV, Swarup S, Hoyer MJ, Paulo JA, and Harper JW (2021). Quantitative proteomics reveals the selectivity of ubiquitin-binding autophagy receptors in the turnover of damaged lysosomes by lysophagy. Elife 10, e72328. 10.7554/eLife.72328. [PubMed: 34585663]

19. Liu EA, Schultz ML, Mochida C, Chung C, Paulson HL, and Lieberman AP (2020). Fbxo2 mediates clearance of damaged lysosomes and modifies neurodegeneration in the Niemann-Pick C brain. JCI Insight 5, e136676. 10.1172/jci.insight.136676. [PubMed: 32931479]

20. Radulovic M, Schink KO, Wenzel EM, Nähse V, Bongiovanni A, Lafont F, and Stenmark H (2018). ESCRT -mediated lysosome repair precedes lysophagy and promotes cell survival. EMBO J. 37, e99753. 10.15252/embj.201899753. [PubMed: 30314966]

21. Skowyra ML, Schlesinger PH, Naismith TV, and Hanson PI (2018). Triggered recruitment of ESCRT machinery promotes endolysosomal repair. Science 360, eaar5078. 10.1126/science.aar5078. [PubMed: 29622626]

22. Jia J, Claude-Taupin A, Gu Y, Choi SW, Peters R, Bissa B, Mudd MH, Allers L, Pallikkuth S, Lidke KA, et al. (2020). Galectin-3 coordinates a cellular system for lysosomal repair and removal. Dev. Cell 52, 69–87.e8. 10.1016/j.devcel.2019.10.025. [PubMed: 31813797]

23. Chen R-H, Chen Y-H, and Huang T-Y (2019). Ubiquitin-mediated regulation of autophagy. J. Biomed. Sci 26, 80. 10.1186/s12929-019-0569-y. [PubMed: 31630678]

24. Khaminets A, Behl C, and Dikic I (2016). Ubiquitin-dependent and independent signals in selective autophagy. Trends Cell Biol. 26, 6–16. 10.1016/j.tcb.2015.08.010. [PubMed: 26437584]

25. Stolz A, Ernst A, and Dikic I (2014). Cargo recognition and trafficking in selective autophagy. Nat. Cell Biol 16, 495–501. 10.1038/ncb2979. [PubMed: 24875736]

26. Chauhan S, Kumar S, Jain A, Ponpuak M, Mudd MH, Kimura T, Choi SW, Peters R, Mandell M, Bruun J-A, et al. (2016). TRIMs and galectins globally cooperate and TRIM16 and galectin-3 Co-direct autophagy in endomembrane damage homeostasis. Dev. Cell 39, 13–27. 10.1016/j.devcel.2016.08.003. [PubMed: 27693506]

27. Di Rienzo M, Romagnoli A, Antonioli M, Piacentini M, and Fimia GM (2020). TRIM proteins in autophagy: selective sensors in cell damage and innate immune responses. Cell Death Differ. 27, 887–902. 10.1038/s41418-020-0495-2. [PubMed: 31969691]

28. Maejima I, Takahashi A, Omori H, Kimura T, Takabatake Y, Saitoh T, Yamamoto A, Hamasaki M, Noda T, Isaka Y, et al. (2013). Autophagy sequesters damaged lysosomes to control lysosomal biogenesis and kidney injury. EMBO J. 32, 2336–2347. 10.1038/emboj.2013.171. [PubMed: 23921551]

29. Papadopoulos C, and Meyer H (2017). Detection and clearance of damaged lysosomes by the endo-lysosomal damage response and lysophagy. Curr. Biol 27, R1330–R1341. 10.1016/j.cub.2017.11.012. [PubMed: 29257971]

30. Papadopoulos C, Kirchner P, Bug M, Grum D, Koerver L, Schulze N, Poehler R, Dressler A, Fengler S, Arhzaouy K, et al. (2017). VCP/p97 cooperates with YOD 1, UBXD 1 and

PLAA to drive clearance of ruptured lysosomes by autophagy. EMBO J. 36, 135–150. 10.15252/embj.201695148. [PubMed: 27753622]

31. Fujita N, Morita E, Itoh T, Tanaka A, Nakaoka M, Osada Y, Umemoto T, Saitoh T, Nakatogawa H, Kobayashi S, et al. (2013). Recruitment of the autophagic machinery to endosomes during infection is mediated by ubiquitin. J. Cell Biol 203, 115–128. 10.1083/jcb.201304188. [PubMed: 24100292]
32. Hung Y-H, Chen LM-W, Yang J-Y, and Yang WY (2013). Spatiotemporally controlled induction of autophagy-mediated lysosome turnover. Nat. Commun 4, 2111. 10.1038/ncomms3111. [PubMed: 23817530]
33. Koerver L, Papadopoulos C, Liu B, Kravic B, Rota G, Brecht L, Veenendaal T, Polajnar M, Bluemke A, Ehrmann M, et al. (2019). The ubiquitin-conjugating enzyme UBE 2 QL 1 coordinates lysophagy in response to endolysosomal damage. EMBO Rep. 20, e48014. 10.15252/embr.201948014. [PubMed: 31432621]
34. Yoshida Y, Yasuda S, Fujita T, Hamasaki M, Murakami A, Kawawaki J, Iwai K, Saeki Y, Yoshimori T, Matsuda N, et al. (2017). Ubiquitination of exposed glycoproteins by SCF^{FBXO27} directs damaged lysosomes for autophagy. Proc. Natl. Acad. Sci. USA 114, 8574–8579. 10.1073/pnas.1702615114. [PubMed: 28743755]
35. Ravenhill BJ, Boyle KB, von Muhlinen N, Ellison CJ, Masson GR, Otten EG, Foeglein A, Williams R, and Randow F (2019). The cargo receptor NDP52 initiates selective autophagy by recruiting the ULK complex to cytosol-invading bacteria. Mol. Cell 74, 320–329.e6. 10.1016/j.molcel.2019.01.041. [PubMed: 30853402]
36. Sun D, Wu R, Zheng J, Li P, and Yu L (2018). Polyubiquitin chain-induced p62 phase separation drives autophagic cargo segregation. Cell Res. 28, 405–415. 10.1038/s41422-018-0017-7. [PubMed: 29507397]
37. Turco E, Witt M, Abert C, Bock-Bierbaum T, Su M-Y, Trapannone R, Sztacho M, Danieli A, Shi X, Zaffagnini G, et al. (2019). FIP200 claw domain binding to p62 promotes autophagosome formation at ubiquitin condensates. Mol. Cell 74, 330–346.e11. 10.1016/j.molcel.2019.01.035. [PubMed: 30853400]
38. Peng SZ, Chen XH, Chen SJ, Zhang J, Wang CY, Liu WR, Zhang D, Su Y, and Zhang XK (2021). Phase separation of Nur77 mediates celastrol-induced mitophagy by promoting the liquidity of p62/SQSTM1 condensates. Nat. Commun 12, 5989. 10.1038/s41467-021-26295-8. [PubMed: 34645818]
39. Narendra D, Kane LA, Hauser DN, Fearnley IM, and Youle RJ (2010). p62/SQSTM1 is required for Parkin-induced mitochondrial clustering but not mitophagy; VDAC1 is dispensable for both. Autophagy 6, 1090–1106. 10.4161/auto.6.8.13426. [PubMed: 20890124]
40. Wong YC, and Holzbaur ELF (2014). Optineurin is an autophagy receptor for damaged mitochondria in parkin-mediated mitophagy that is disrupted by an ALS-linked mutation. Proc. Natl. Acad. Sci. USA 111, E4439–E4448. 10.1073/pnas.1405752111. [PubMed: 25294927]
41. Abu-Remaileh M, Wyant GA, Kim C, Laqtom NN, Abbasi M, Chan SH, Freinkman E, and Sabatini DM (2017). Lysosomal metabolomics reveals V-ATPase- and mTOR-dependent regulation of amino acid efflux from lysosomes. Science 358, 807–813. 10.1126/science.aan6298. [PubMed: 29074583]
42. Jia J, Abudu YP, Claude-Taupin A, Gu Y, Kumar S, Choi SW, Peters R, Mudd MH, Allers L, Salemi M, et al. (2018). Galectins control mTOR in response to endomembrane damage. Mol. Cell 70, 120–135.e8. 10.1016/j.molcel.2018.03.009. [PubMed: 29625033]
43. Jia J, Bissa B, Brecht L, Allers L, Choi SW, Gu Y, Zbinden M, Burge MR, Timmins G, Hallows K, et al. (2020). AMPK, a regulator of metabolism and autophagy, is activated by lysosomal damage via a novel galectin-directed ubiquitin signal transduction system. Mol. Cell 77, 951–969.e9. 10.1016/j.molcel.2019.12.028. [PubMed: 31995728]
44. Thiele DL, and Lipsky PE (1990). Mechanism of L-leucyl-L-leucine methyl ester-mediated killing of cytotoxic lymphocytes: dependence on a lysosomal thiol protease, dipeptidyl peptidase I, that is enriched in these cells. Proc. Natl. Acad. Sci. USA 87, 83–87. 10.1073/pnas.87.1.83. [PubMed: 2296607]

45. Villamil Giraldo AM, Appelqvist H, Ederth T, and Øllinger K (2014). Lysosomotropic agents: impact on lysosomal membrane permeabilization and cell death. Biochem. Soc. Trans 42, 1460–1464. 10.1042/BST20140145. [PubMed: 25233432]
46. Fukuda M, Viitala J, Matteson J, and Carlsson SR (1988). Cloning of cDNAs encoding human lysosomal membrane glycoproteins, h-lamp-1 and h-lamp-2. Comparison of their deduced amino acid sequences. J. Biol. Chem 268, 18920–18928. 10.1016/S0021-9258(18)37370-8.
47. Bulina ME, Chudakov DM, Britanova OV, Yanushevich YG, Staroverov DB, Chepurnykh TV, Merzlyak EM, Shkrob MA, Lukyanov S, and Lukyanov KA (2006). A genetically encoded photosensitizer. Nat. Biotechnol. 24, 95–99. 10.1038/nbt1175. [PubMed: 16369538]
48. Boecker CA, Olenick MA, Gallagher ER, Ward ME, and Holzbaur ELF (2020). ToolBox: live Imaging of intracellular organelle transport in induced pluripotent stem cell-derived neurons. Traffic 21, 138–155. 10.1111/tra.12701. [PubMed: 31603614]
49. Fernandopulle MS, Prestil R, Grunseich C, Wang C, Gan L, and Ward ME (2018). Transcription factor-mediated differentiation of human iPSCs into neurons: rapid differentiation of iPSCs into neurons. Curr. Protoc. Cell Biol 79, e51. 10.1002/cpcb.51. [PubMed: 29924488]
50. Aits S, Kricker J, Liu B, Ellegaard A-M, Hämälistö S, Tvingsholm S, Corcelle-Termeau E, Høgh S, Farkas T, Holm Jonassen A, et al. (2015). Sensitive detection of lysosomal membrane permeabilization by lysosomal galectin puncta assay. Autophagy 11, 1408–1424. 10.1080/15548627.2015.1063871. [PubMed: 26114578]
51. Lin CY, Nozawa T, Minowa-Nozawa A, Toh H, Aikawa C, and Nakagawa I (2019). LAMTOR2/LAMTOR1 complex is required for TAX1BP1-mediated xenophagy. Cell Microbiol. 21, e12981. 10.1111/cmi.12981. [PubMed: 30428163]
52. Sancak Y, Bar-Peled L, Zoncu R, Markhard AL, Nada S, and Sabatini DM (2010). Ragulator-rag complex targets mTORC1 to the lysosomal surface and is necessary for its activation by amino acids. Cell 141, 290–303. 10.1016/j.cell.2010.02.024. [PubMed: 20381137]
53. Lazarou M, Sliter DA, Kane LA, Sarraf SA, Wang C, Burman JL, Sideris DP, Fogel AI, and Youle RJ (2015). The ubiquitin kinase PINK1 recruits autophagy receptors to induce mitophagy. Nature 524, 309–314. 10.1038/nature14893. [PubMed: 26266977]
54. Lamark T, Perander M, Outzen H, Kristiansen K, Øvervatn A, Michaelsen E, Bjørkøy G, and Johansen T (2003). Interaction codes within the family of mammalian Phox and Bem1p domain-containing proteins. J. Biol. Chem 278, 34568–34581. 10.1074/jbc.M303221200. [PubMed: 12813044]
55. Yim WW-Y, Yamamoto H, and Mizushima N (2022). A pulse-chasable reporter processing assay for mammalian autophagic flux with HaloTag. Elife 11, e78923. 10.7554/eLife.78923. [PubMed: 35938926]
56. Yoshimori T, Yamamoto A, Moriyama Y, Futai M, and Tashiro Y (1991). Bafilomycin A1, a specific inhibitor of vacuolar-type H(+)-ATPase, inhibits acidification and protein degradation in lysosomes of cultured cells. J. Biol. Chem 266, 17707–17712. [PubMed: 1832676]
57. Seibenhener ML, Babu JR, Geetha T, Wong HC, Krishna NR, and Wooten MW (2004). Sequestosome 1/p62 is a polyubiquitin chain binding protein involved in ubiquitin proteasome degradation. Mol. Cell Biol 24, 8055–8068. 10.1128/MCB.24.18.8055-8068.2004. [PubMed: 15340068]
58. Johansen T, and Lamark T (2011). Selective autophagy mediated by autophagic adapter proteins. Autophagy 7, 279–296. 10.4161/auto.7.3.14487. [PubMed: 21189453]
59. Pankiv S, Clausen TH, Lamark T, Brech A, Bruun J-A, Outzen H, Øvervatn A, Bjørkøy G, and Johansen T (2007). p62/SQSTM1 binds directly to atg8/LC3 to facilitate degradation of ubiquitinated protein aggregates by autophagy. J. Biol. Chem 282, 24131–24145. 10.1074/jbc.M702824200. [PubMed: 17580304]
60. Wurzer B, Zaffagnini G, Fracchiolla D, Turco E, Abert C, Romanov J, and Martens S (2015). Oligomerization of p62 allows for selection of ubiquitinated cargo and isolation membrane during selective autophagy. Elife 4, e08941. 10.7554/eLife.08941. [PubMed: 26413874]
61. Wilson MI, Gill DJ, Perisic O, Quinn MT, and Williams RL (2003). PB1 domain-mediated heterodimerization in NADPH oxidase and signaling complexes of atypical protein kinase C with Par6 and p62. Mol. Cell 12, 39–50. 10.1016/S1097-2765(03)00246-6. [PubMed: 12887891]

62. Turco E, Fischer I, and Martens S (2020). FIP200 organizes the autophagy machinery at p62-ubiquitin condensates beyond activation of the ULK1 kinase. Preprint at bioRxiv. 10.1101/2020.07.07.191189.

63. Jakobi AJ, Huber ST, Mortensen SA, Schultz SW, Palara A, Kuhm T, Shrestha BK, Lamark T, Hagen WJH, Wilmanns M, et al. (2020). Structural basis of p62/SQSTM1 helical filaments and their role in cellular cargo uptake. Nat. Commun 11, 440. 10.1038/s41467-020-14343-8. [PubMed: 31974402]

64. Kageyama S, Gudmundsson SR, Sou Y-S, Ichimura Y, Tamura N, Kazuno S, Ueno T, Miura Y, Noshiro D, Abe M, et al. (2021). p62/SQSTM1-droplet serves as a platform for autophagosome formation and anti-oxidative stress response. Nat. Commun 12, 16. 10.1038/s41467-020-20185-1. [PubMed: 33397898]

65. Haidar M, Asselbergh B, Adriaenssens E, De Winter V, Timmermans J-P, Auer-Grumbach M, Juneja M, and Timmerman V (2019). Neuropathy-causing mutations in HSPB1 impair autophagy by disturbing the formation of SQSTM1/p62 bodies. Autophagy 15, 1051–1068. 10.1080/15548627.2019.1569930. [PubMed: 30669930]

66. Liu Z, Zhang S, Gu J, Tong Y, Li Y, Gui X, Long H, Wang C, Zhao C, Lu J, et al. (2020). Hsp27 chaperones FUS phase separation under the modulation of stress-induced phosphorylation. Nat. Struct. Mol. Biol 27, 363–372. 10.1038/s41594-020-0399-3. [PubMed: 32231288]

67. Lu S, Hu J, Arogundade OA, Goginashvili A, Vazquez-Sanchez S, Diedrich JK, Gu J, Blum J, Oung S, Ye Q, et al. (2022). Heat-shock chaperone HSPB1 regulates cytoplasmic TDP-43 phase separation and liquid-to-gel transition. Nat. Cell Biol 24, 1378–1393. 10.1038/s41556-022-00988-8. [PubMed: 36075972]

68. Landry J, Lambert H, Zhou M, Lavoie JN, Hickey E, Weber LA, and Anderson CW (1992). Human HSP27 is phosphorylated at serines 78 and 82 by heat shock and mitogen-activated kinases that recognize the same amino acid motif as S6 kinase II. J. Biol. Chem 267, 794–803. 10.1016/S0021-9258(18)48354-8. [PubMed: 1730670]

69. Niswander JM, and Dokas LA (2006). Phosphorylation of HSP27 and synthesis of 14-3-3ε are parallel responses to hyperosmotic stress in the hippocampus. Brain Res. 1116, 19–30. 10.1016/j.brainres.2006.07.119. [PubMed: 16950235]

70. Yang C, Wang H, Zhu D, Hong CS, Dmitriev P, Zhang C, Li Y, Ikejiri B, Brady RO, and Zhuang Z (2015). Mutant glucocerebrosidase in Gaucher disease recruits Hsp27 to the Hsp90 chaperone complex for proteasomal degradation. Proc. Natl. Acad. Sci. USA 112, 1137–1142. 10.1073/pnas.1424288112. [PubMed: 25583479]

71. Axe EL, Walker SA, Manifava M, Chandra P, Roderick HL, Habermann A, Griffiths G, and Ktistakis NT (2008). Autophagosome formation from membrane compartments enriched in phosphatidylinositol 3-phosphate and dynamically connected to the endoplasmic reticulum. J. Cell Biol 182, 685–701. 10.1083/jcb.200803137. [PubMed: 18725538]

72. Yamasaki A, Alam JM, Noshiro D, Hirata E, Fujioka Y, Suzuki K, Ohsumi Y, and Noda NN (2020). Liquidity is a critical determinant for selective autophagy of protein condensates. Mol. Cell 77, 1163–1175.e9. 10.1016/j.molcel.2019.12.026. [PubMed: 31995729]

73. Carisey A, Stroud M, Tsang R, and Ballestrem C (2011). Fluorescence recovery after photobleaching. In Cell Migration Methods in Molecular Biology, Wells CM and Parsons M, eds. (Humana Press), pp. 387–402. 10.1007/978-1-61779-207-6_26.

74. Al-Sarraj S, King A, Troakes C, Smith B, Maekawa S, Bodi I, Rogelj B, Al-Chalabi A, Hortobágyi T, and Shaw CE (2011). p62 positive, TDP-43 negative, neuronal cytoplasmic and intranuclear inclusions in the cerebellum and hippocampus define the pathology of C9orf72-linked FTLD and MND/ALS. Acta Neuropathol. 722, 691–702. 10.1007/s00401-011-0911-2.

75. Foster AD, Flynn LL, Cluning C, Cheng F, Davidson JM, Lee A, Polain N, Mejzini R, Farrawell N, Yerbury JJ, et al. (2021). p62 overexpression induces TDP-43 cytoplasmic mislocalisation, aggregation and cleavage and neuronal death. Sci. Rep 11, 11474. 10.1038/s41598-021-90822-2. [PubMed: 34075102]

76. Mitsui S, Otomo A, Nozaki M, Ono S, Sato K, Shirakawa R, Adachi H, Aoki M, Sobue G, Shang H-F, et al. (2018). Systemic overexpression of SQSTM1/p62 accelerates disease onset in a SOD1H46R-expressing ALS mouse model. Mol. Brain 11, 30. 10.1186/s13041-018-0373-8. [PubMed: 29843805]

77. Teyssou E, Takeda T, Lebon V, Boillée S, Doukouré B, Bataillon G, Sazdovitch V, Cazeneuve C, Meininger V, LeGuern E, et al. (2013). Mutations in SQSTM1 encoding p62 in amyotrophic lateral sclerosis: genetics and neuropathology. Acta Neuropathol. 125, 511–522. 10.1007/s00401-013-1090-0. [PubMed: 23417734]

78. Fecto F, Yan J, Vemula SP, Liu E, Yang Y, Chen W, Zheng JG, Shi Y, Siddique N, Arrat H, et al. (2011). SQSTM1 mutations in familial and sporadic amyotrophic lateral sclerosis. Arch. Neurol 68, 1440–1446. 10.1001/archneurol.2011.250. [PubMed: 22084127]

79. Chen Y, Zheng Z-Z, Chen X, Huang R, Yang Y, Yuan L, Pan L, Hadano S, and Shang H-F (2014). SQSTM1 mutations in Han Chinese populations with sporadic amyotrophic lateral sclerosis. Neurobiol. Aging 35, 726.e7–726.e9. 10.1016/j.neurobiolaging.2013.09.008.

80. Ichimura Y, Kumanomidou T, Sou Y.s., Mizushima T, Ezaki J, Ueno T, Kominami E, Yamane T, Tanaka K, and Komatsu M (2008). Structural basis for sorting mechanism of p62 in selective autophagy. J. Biol. Chem 283, 22847–22857. 10.1074/jbc.M802182200. [PubMed: 18524774]

81. Goode A, Butler K, Long J, Cavey J, Scott D, Shaw B, Sollenberger J, Gell C, Johansen T, Oldham NJ, et al. (2016). Defective recognition of LC3B by mutant SQSTM1/p62 implicates impairment of autophagy as a pathogenic mechanism in ALS-FTLD. Autophagy 12, 1094–1104. 10.1080/15548627.2016.1170257. [PubMed: 27158844]

82. Cavey JR, Ralston SH, Sheppard PW, Ciani B, Gallagher TRA, Long JE, Searle MS, and Layfield R (2006). Loss of ubiquitin binding is a unifying mechanism by which mutations of SQSTM1 cause paget's disease of bone. Calcif. Tissue Int 78, 271–277. 10.1007/s00223-005-1299-6. [PubMed: 16691492]

83. Deng Z, Lim J, Wang Q, Purtell K, Wu S, Palomo GM, Tan H, Manfredi G, Zhao Y, Peng J, et al. (2020). ALS-FTLD-linked mutations of SQSTM1/p62 disrupt selective autophagy and NFE2L2/NRF2 anti-oxidative stress pathway. Autophagy 16, 917–931. 10.1080/15548627.2019.1644076. [PubMed: 31362587]

84. Garner TP, Long J, Layfield R, and Searle MS (2011). Impact of p62/SQSTM1 UBA domain mutations linked to paget's disease of bone on ubiquitin recognition. Biochemistry 50, 4665–4674. 10.1021/bi200079n. [PubMed: 21517082]

85. Dooley HC, Razi M, Polson HEJ, Girardin SE, Wilson MI, and Tooze SA (2014). WIPI2 links LC3 conjugation with PI3P, autophagosome formation, and pathogen clearance by recruiting atg12–5-16l1. Mol. Cell 55, 238–252. 10.1016/j.molcel.2014.05.021. [PubMed: 24954904]

86. Pilli M, Arko-Mensah J, Ponpuak M, Roberts E, Master S, Mandell MA, Dupont N, Ornatowski W, Jiang S, Bradfute SB, et al. (2012). TBK-1 promotes autophagy-mediated antimicrobial defense by controlling autophagosome maturation. Immunity 37, 223–234. 10.1016/j.immuni.2012.04.015. [PubMed: 22921120]

87. Evgrafov OV, Mersiyanova I, Irobi J, Van Den Bosch L, Dierick I, Leung CL, Schagina O, Verpoorten N, Van Impe K, Fedotov V, et al. (2004). Mutant small heat-shock protein 27 causes axonal Charcot-Marie-Tooth disease and distal hereditary motor neuropathy. Nat. Genet 36, 602–606. 10.1038/ng1354. [PubMed: 15122254]

88. Kravić B, Bionda T, Siebert A, Gahlot P, Levantovsky S, Behrends C, and Meyer H (2022). Ubiquitin profiling of lysophagy identifies actin stabilizer CNN2 as a target of VCP/p97 and uncovers a link to HSPB1. Mol. Cell 82, 2633–2649.e7. 10.1016/j.molcel.2022.06.012. [PubMed: 35793674]

89. Milicevic K, Rankovic B, Andjus PR, Bataveljic D, and Milovanovic D (2022). Emerging roles for phase separation of RNA-binding proteins in cellular pathology of ALS. Front. Cell Dev. Biol 10, 840256. 10.3389/fcell.2022.840256. [PubMed: 35372329]

90. Faruk MO, Ichimura Y, Kageyama S, Komatsu-Hirota S, El-Gowily AH, Sou YS, Koike M, Noda NN, and Komatsu M (2021). Phase-separated protein droplets of amyotrophic lateral sclerosis-associated p62/SQSTM1 mutants show reduced inner fluidity. J. Biol. Chem 297, 101405. 10.1016/j.jbc.2021.101405. [PubMed: 34774801]

91. Kumar AV, Mills J, and Lapierre LR (2022). Selective autophagy receptor p62/SQSTM1, a pivotal player in stress and aging. Front. Cell Dev. Biol 10, 793328. 10.3389/fcell.2022.793328. [PubMed: 35237597]

92. Voss OH, Batra S, Kolattukudy SJ, Gonzalez-Mejia ME, Smith JB, and Doseff AI (2007). Binding of caspase-3 prodomain to heat shock protein 27 regulates monocyte apoptosis by inhibiting

caspase-3 proteolytic activation. J. Biol. Chem 282, 25088–25099. 10.1074/jbc.M701740200. [PubMed: 17597071]

93. Moore AS, and Holzbaur ELF (2016). Dynamic recruitment and activation of ALS-associated TBK1 with its target optineurin are required for efficient mitophagy. Proc. Natl. Acad. Sci. USA 113, E3349–E3358. 10.1073/pnas.1523810113. [PubMed: 27247382]
94. Stavoe AK, Gopal PP, Gubas A, Tooze SA, and Holzbaur EL (2019). Expression of WIPI2B counteracts age-related decline in autophagosome biogenesis in neurons. Elife 8, e44219. 10.7554/eLife.44219. [PubMed: 31309927]
95. Bar-Peled L, Schweitzer LD, Zoncu R, and Sabatini DM (2012). Ragulator is a GEF for the rag GTPases that signal amino acid levels to mTORC1. Cell 150, 1196–1208. 10.1016/j.cell.2012.07.032. [PubMed: 22980980]
96. Fu M, Nirschl JJ, and Holzbaur ELF (2014). LC3 binding to the scaffolding protein JIP1 regulates processive dynein-driven transport of autophagosomes. Dev. Cell 29, 577–590. 10.1016/j.devcel.2014.04.015. [PubMed: 24914561]
97. Itakura E, and Mizushima N (2011). p62 targeting to the autophagosome formation site requires self-oligomerization but not LC3 binding. J. Cell Biol 192, 17–27. 10.1083/jcb.201009067. [PubMed: 21220506]
98. Berg S, Kutra D, Kroeger T, Straehle CN, Kausler BX, Haubold C, Schiegg M, Ales J, Beier T, Rudy M, et al. (2019). ilastik: interactive machine learning for (bio)image analysis. Nat. Methods 16, 1226–1232. 10.1038/s41592-019-0582-9. [PubMed: 31570887]
99. Deosaran E, Larsen KB, Hua R, Sargent G, Wang Y, Kim S, Lamark T, Jauregui M, Law K, Lippincott-Schwartz J, et al. (2013). NBR1 acts as an autophagy receptor for peroxisomes. J. Cell Sci 126, 939–952. 10.1242/jcs.114819. [PubMed: 23239026]
100. Sherer NM, Lehmann MJ, Jimenez-Soto LF, Ingmundson A, Horner SM, Cicchetti G, Allen PG, Pypaert M, Cunningham JM, and Mothes W (2003). Visualization of retroviral replication in living cells reveals budding into multivesicular bodies: retroviral budding. Traffic 4, 785–801. 10.1034/j.1600-0854.2003.00135.x. [PubMed: 14617360]
101. Itakura E, and Mizushima N (2010). Characterization of autophagosome formation site by a hierarchical analysis of mammalian Atg proteins. Autophagy 6, 764–776. 10.4161/auto.6.6.12709. [PubMed: 20639694]
102. Kabeya Y, Mizushima N, Ueno T, Yamamoto A, Kirisako T, Noda T, Kominami E, Ohsumi Y, and Yoshimori T (2000). LC3, a mammalian homologue of yeast Apg8p, is localized in autophagosome membranes after processing. EMBO J. 19, 5720–5728. 10.1093/emboj/19.21.5720. [PubMed: 11060023]
103. Stewart SA, Dykxhoorn DM, Palliser D, Mizuno H, Yu EY, An DS, Sabatini DM, Chen ISY, Hahn WC, Sharp PA, et al. (2003). Lentivirus-delivered stable gene silencing by RNAi in primary cells. RNA 9, 493–501. 10.1261/rna.2192803. [PubMed: 12649500]
104. Lord SJ, Velle KB, Mullins RD, and Fritz-Laylin LK (2020). Super-Plots: communicating reproducibility and variability in cell biology. J. Cell Biol 219, e202001064. 10.1083/jcb.202001064. [PubMed: 32346721]
105. Otsu N (1979). A threshold selection method from gray-level histograms. IEEE Trans. Syst. Man Cybern 9, 62–66. 10.1109/TSMC.1979.4310076.
106. Reits EA, and Neefjes JJ (2001). From fixed to FRAP: measuring protein mobility and activity in living cells. Nat. Cell Biol 3, E145–E147. 10.1038/35078615. [PubMed: 11389456]

Highlights

- p62/SQSTM1 is recruited to damaged lysosomes in HeLa cells and neurons
- Lysophagy requires p62 recruitment and oligomerization
- p62 recruits HSP27 to lysosomes after damage-induced phosphorylation of HSP27
- Lysophagy requires HSP27 to regulate p62 condensates at damaged lysosomes

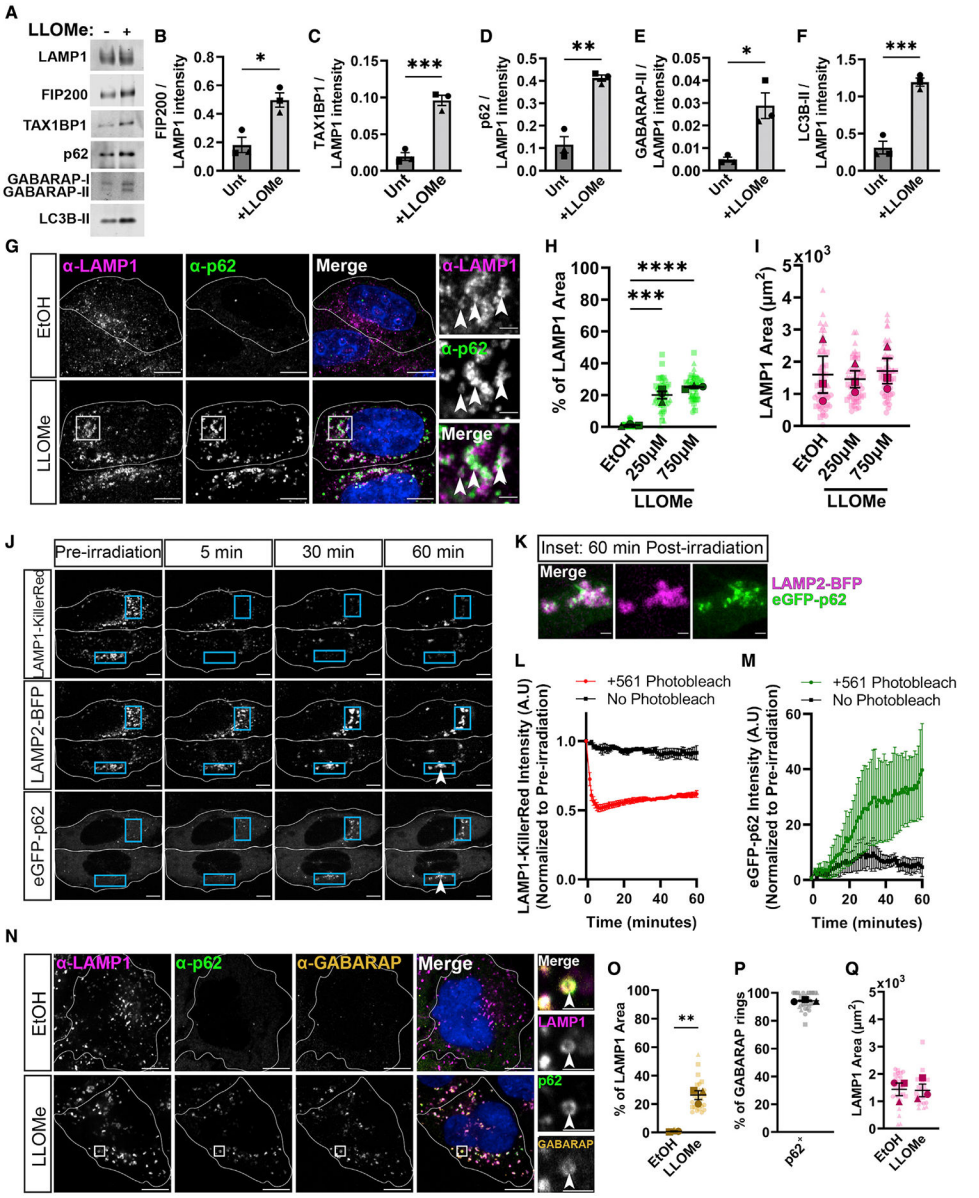

Figure 1. p62 is dynamically recruited to damaged lysosomes in HeLa cells

(A) Western blot analysis of lysosomal immunoprecipitation following either no treatment (−) or treatment with 1.0 mM LLOMe (+) for 1 h.

(B–F) Quantification of lysosomal immunoprecipitation following normalization to α-LAMP1 intensity in either untreated (Unt) or LLOMe-treated HeLa cells. (B) α-FIP200 band intensities (unpaired t test, $p < 0.05$, $n = 3$). (C) α-TAX1BP1 band intensities (unpaired t test, $p < 0.001$, $n = 3$). (D) α-p62 band intensities (unpaired t test, $p < 0.01$, $n = 3$). (E) α-GABARAP band intensities (unpaired t test, $p < 0.05$, $n = 3$). (F) α-LC3B band intensities (unpaired t test, $p < 0.001$, $n = 3$).

(G) Single z-plane representative images of endogenous α-LAMP1 and α-p62 in HeLa cells treated with ethanol (EtOH) as a vehicle control or LLOMe (at 250 or 750 μM) for 2 h. Cell

outlines are traced. White boxes indicate inset image region. Arrowheads indicate regions of co-localization. Scale bars (SB): 10 μm; insets: 2 μm.

(H) Quantification of the overlapping area from maximum (max) projections between endogenous α-p62 and α-LAMP1 in cells treated with EtOH or different concentrations of LLOMe (one-way ANOVA, $p_{(EtOH/250)} < 0.001$, $p_{(EtOH/750)} < 0.0001$, n = 3 experiments. Number of cells analyzed per condition ≥ 54).

(I) Quantification of LAMP1 area from max projections for the experiments shown in (H) (one-way ANOVA, $p_{(EtOH/250)} = 0.96$, $p_{(EtOH/750)} = 0.9766$, n = 3 experiments. Number of cells analyzed per condition ≥ 54).

(J) Representative images of HeLa cells transiently transfected with LAMP1-KillerRed, LAMP2-BFP, and EGFP-p62. Cell outlines are traced. Blue boxes reflect regions irradiated. Arrowheads reflect location of inset images in (K). SBs: 10 μm.

(K) Inset images from (J), showing EGFP-p62 recruitment to lysosomes in HeLa cells at 60 min post-laser irradiation. SBs: 2 μm.

(L) Quantification of LAMP1-KillerRed intensities within irradiated or Unt regions from the same cells.

(M) Quantification of EGFP-p62 intensities within irradiated or Unt regions.

(N) Single z-plane representative images of endogenous α-LAMP1, α-p62, and α-GABARAP/L1/L2 in HeLa cells, which were treated with EtOH or 750 μM LLOMe for 2 h. Cell outlines are traced. White boxes indicate inset region. Arrowheads in inset regions indicate co-localization. SBs: 10 αm; insets: 2 αm.

(O) Quantification of the percentage of α-LAMP1 occupied by α-GABARAPs (unpaired t test, $p < 0.01$, n = 3 experiments. Number of cells analyzed per condition ≥ 29).

(P) Quantification of the percentage of α-GABARAPs rings (in single z-plane) co-localizing with α-p62 (% $p62^+$: 94% ± 0.49%). Data are represented as mean ± SEM.

(Q) Quantification of α-LAMP1 area per cell (unpaired t test, $p = 0.9117$, n = 3 experiments. Number of cells analyzed per condition ≥ 29).

All error bars reflect mean ± SEM. See also Video S1.

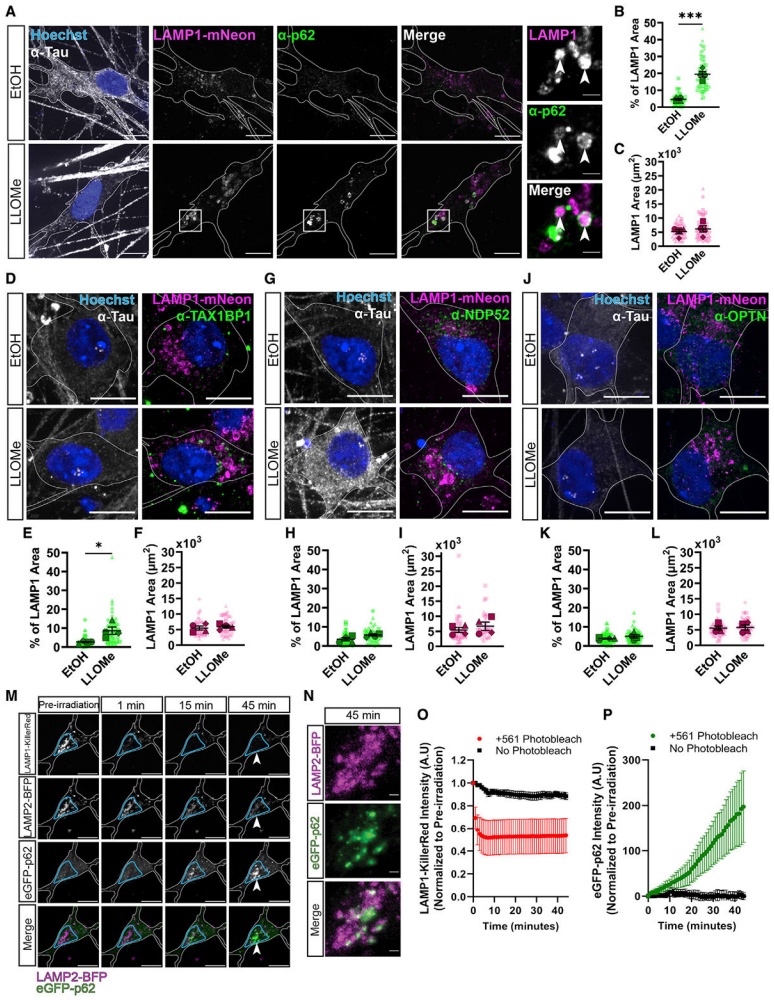

Figure 2. p62 responds to lysosomal damage in human and rat neurons

(A) Representative max projections of α-p62 and LAMP1-mNeonGreen in human iPSC-derived neurons (i^{3}Neurons), which were treated with EtOH or 1.0 mM LLOMe for 2 h. Cell outlines are traced. White boxes indicate inset image region. Arrowheads indicate areas of co-localization. Inset images are single z-plane images. SBs: 10 αm; insets: 2 αm.

(B) Quantification of the overlapping area from max projections between α-p62 and LAMP1-mNeonGreen in cells treated with EtOH or with LLOMe (unpaired t test, $p < 0.001$, n = 4 experiments. Number of cells analyzed per condition ≥ 54).

(C) Quantification of LAMP1 area from max projections in the different conditions (unpaired t test, $p = 0.5047$, n = 4 experiments. Number of cells analyzed per condition ≥ 54).

(D) Representative max projections of images comparing α-TAX1BP1 localization with lysosomes in i^{3}Neurons following treatment with either EtOH or 1.0 mM LLOMe for 2 h. Cell outlines were traced. SBs: 10 αm.

(E) Quantification of the percentage of LAMP1 area occupied by α-TAX1BP1in cells treated with EtOH or with LLOMe (unpaired t test, $p < 0.05$, n = 4 experiments. Number of cells analyzed per condition ≥ 45).

(F) Quantification of LAMP1 area from max projections in the different conditions (unpaired t test, p = 0.6003, n = 4 experiments. Number of cells analyzed per condition ≥ 45).
(G) Representative max projections of images comparing α-NDP52 localization with lysosomes in i^3Neurons following treatment with either EtOH or 1.0 mM LLOMe for 2 h. Cell outlines were traced. SBs: 10 μm.
(H) Quantification of the percentage of LAMP1 area occupied by α-NDP52 in cells treated with EtOH or with LLOMe (unpaired t test, p = 0.0708, n = 4 experiments. Number of cells analyzed per condition ≥ 45).
(I) Quantification of LAMP1 area from max projections in the different conditions (unpaired t test, p = 0.4643, n = 4 experiments. Number of cells analyzed per condition ≥ 45).
(J) Representative images max projections comparing α-OPTN localization with lysosomes in i^3Neurons following treatment with either EtOH or 1.0 mM LLOMe for 2 h. Cell outlines were traced. SBs: 10 μm.
(K) Quantification of the percentage of LAMP1 area occupied by α-OPTN in cells treated with EtOH or with LLOMe (unpaired t test, p = 0.2476, n = 4 experiments). Number of cells analyzed per condition ≥ 50).
(L) Quantification of LAMP1 area from max projections in the different conditions (unpaired t test, p = 0.8482, n = 4 experiments. Number of cells analyzed per condition ≥ 50).
(M) Representative images of rat hippocampal neurons transiently transfected with LAMP1-KillerRed, LAMP2-BFP, and EGFP-p62. Cell outlines are traced. Blue boxes reflect regions irradiated. Arrowheads reflect location of inset images in Figure 1N. SBs: 10 μm.
(N) Inset images of LAMP2-BFP and EGFP-p62 from Figure 1M of rat hippocampal neurons following 45-min post-laser activation. SBs: 2 μm.
(O) Quantification of LAMP1-KillerRed intensities within irradiated or untreated regions.
(P) Quantification of EGFP-p62 intensities within irradiated or untreated regions.
All error bars reflect mean ± SEM. See also Video S2.

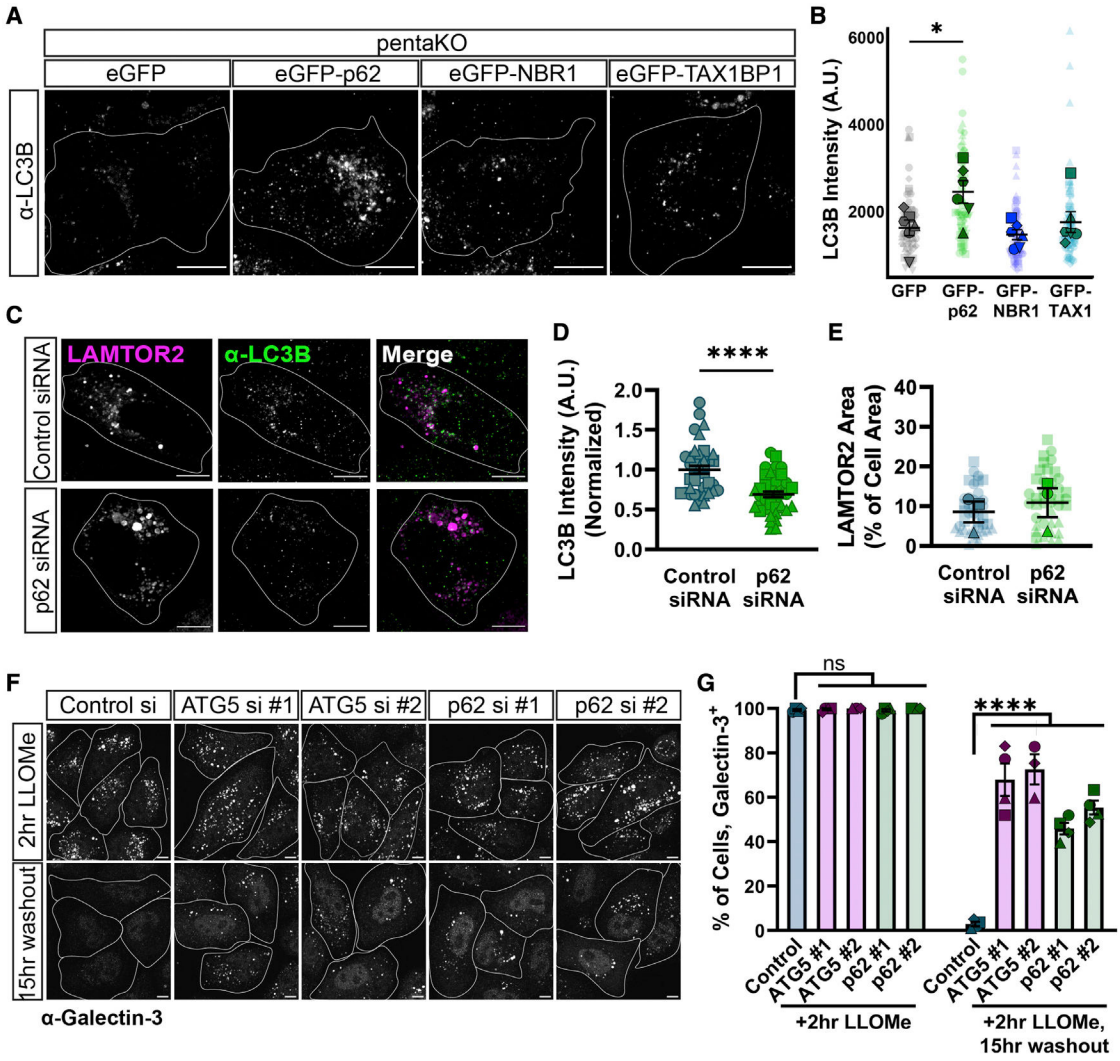

Figure 3. p62 is necessary and sufficient for lysophagy

(A) Representative max projections of α-LC3B in pentaKO HeLa cells. Cells were treated with 750 μM LLOMe for 2 h. Cells were transfected with mCherry-LAMTOR2 and either GFP vector, EGFP-p62, EGFP-NBR1, or EGFP-TAX1BP1; endogenous LC3B was visualized by immunostaining. Cell outlines are traced. SBs: 10 μm.

(B) Quantification of α-LC3B intensity at LAMTOR2 puncta across different conditions (one-way ANOVA, $p_{(GFP/p62)} < 0.05$, $p_{(GFP/NBR1)} = 0.9042$, $p_{(GFP/TAX1)} = 0.9417$, n = 6 experiments, Number of cells analyzed per condition ≥ 64).

(C) Representative max projections of mCherry-LAMTOR2 and α-LC3B in HeLa cells, which were transiently transfected with control siRNA or p62 siRNA (#1) alongside mCherry-LAMTOR2. HeLa cells were treated with 750 μM LLOMe for 2 h. Cell outlines are traced. SBs: 10 μm.

(D) Quantification of normalized α-LC3B intensity at LAMTOR2 puncta across different conditions (Mann-Whitney U test, $p < 0.0001$, n ≥ 40 cells per condition).

(E) Quantification of mCherry-LAMTOR2 area across different conditions (unpaired t test, $p = 0.6338$, n = 3 experiments. Number of cells analyzed per condition ≥ 40).

(F) Representative max projections of endogenous galectin-3 flux assay. Cells were fixed immediately following LLOMe treatment or 15 h post-washout of LLOMe. Cells were transiently transfected with one of two ATG5 siRNAs, one of two p62 siRNAs, or a control siRNA. Cell outlines are traced. SBs: 10 μm.

(G) Quantification of the galectin-3 flux assay, indicating the fraction of cells with n > 3 galectin-3 puncta per cell (one-way ANOVA, post-LLOMe: $p_{(control/ATG5\#1)} > 0.9999$, $p_{(control/ATG5\#2)} > 0.9999$, $p_{(control/p62\#1)} > 0.9999$, $p_{(control/p62\#2)} > 0.9999$; post-washout: $p_{(control/ATG5\#1)} < 0.0001$, $p_{(control/ATG5\#2)} < 0.0001$, $p_{(control/p62\#1)} < 0.0001$, $p_{(control/p62\#2)} < 0.0001$, $p_{(ATG5\ \#1/ATG5\#2)} = 0.9983$, $p_{(p62\ \#1/p62\#2)} = 0.5105$; n = 3 or 4 experiments). All error bars reflect mean ± SEM. See also Figures S1, S2 and S3.

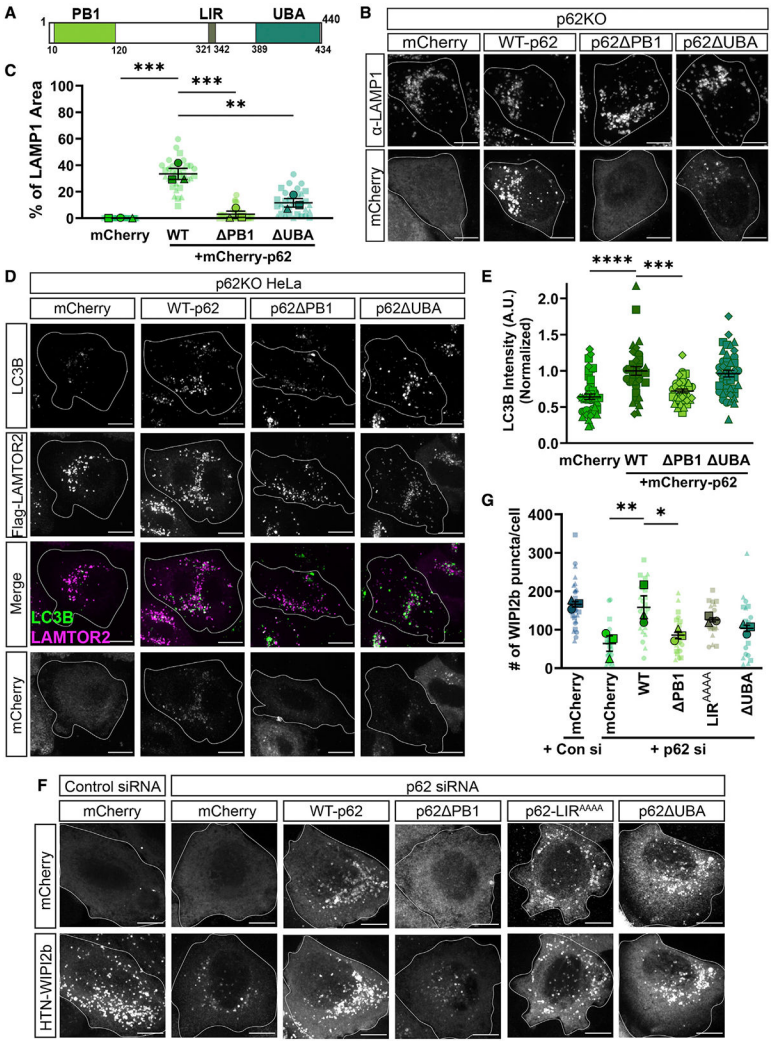

Figure 4. p62 oligomerization is critical in lysophagy

(A) Schematic of p62 domain architecture, highlighting the N-terminal Phox and Bem1p (PB1) domain, LC3-interacting region (LIR), and ubiquitin-associated domain (UBA).

(B) Representative images of α-LAMP1 and either mCherry vector WT-p62, p62ΔPB1, or p62ΔUBA in p62KO HeLa after addition of 750 μM LLOMe for 2 h. Cell outlines are traced. SBs: 10 μm.

(C) Quantification of α-LAMP1 area overlapping with p62 area across different conditions (one-way ANOVA, $p_{(WT/mCherry)} < 0.001$, $p_{(WT/\Delta PB1)} < 0.001$, $p_{(WT/\Delta UBA)} < 0.01$, n = 3 experiments. Number of cells analyzed per condition ≥ 33).

(D) Representative images of α-LC3B in p62KO HeLa, which were transiently transfected with Flag-LAMTOR2 and either mCherry vector, WT-p62, p62ΔPB1, or p62ΔUBA after addition of 750 μM LLOMe for 2 h. Cell outlines are traced. SBs: 10 μm.

(E) Quantification of normalized α-LC3B intensity at FLAG-LAMTOR2 puncta across different conditions (Kruskal-Wallis test, $p_{(WT/mCherry)} < 0.0001$, $p_{(WT/\Delta PB1)} < 0.001$, $p_{(WT/\Delta UBA)} > 0.9999$, $p_{(\Delta UBA/\Delta PB1)} < 0.001$, n = 4 experiments. Number of cells analyzed per condition ≥ 36).

(F) Representative images of mCherry and HaloTag-WIPI2b in HeLa, which were co-transfected with control siRNA or p62 siRNA (#1). Cells were transfected with different mCherry rescue constructs, which were mCherry vector, WT-p62, p62ΔPB1, p62-LIR^{AAAA}, or p62ΔUBA after addition of 750 μM LLOMe for 2 h. Cell outlines are traced. SBs: 10 μm.
(G) Quantification of the number of WIPI2b puncta per cell following LLOMe treatment (one-way ANOVA, $p_{(control\text{-}si+mCherry/p62\text{-}si+mCherry)} < 0.01$ (not depicted), $p_{(control\text{-}si+mCherry/p62\text{-}si+WT)} = 0.9996$, $p_{(p62\text{-}si+WT/p62\text{-}si+mCherry)} < 0.01$, $p_{(p62\text{-}si+WT/p62\text{-}si+\Delta PB1)} < 0.05$, $p_{(p62\text{-}si+WT/p62\text{-}si+LIRmut)} = 0.6880$, $p_{(p62\text{-}si+WT/p62\text{-}si+\Delta UBA)} = 0.1794$, n = 3 experiments. Number of cells analyzed per condition ≥ 20).
All error bars reflect mean ± SEM. See also Figures S3, S4, and S5.

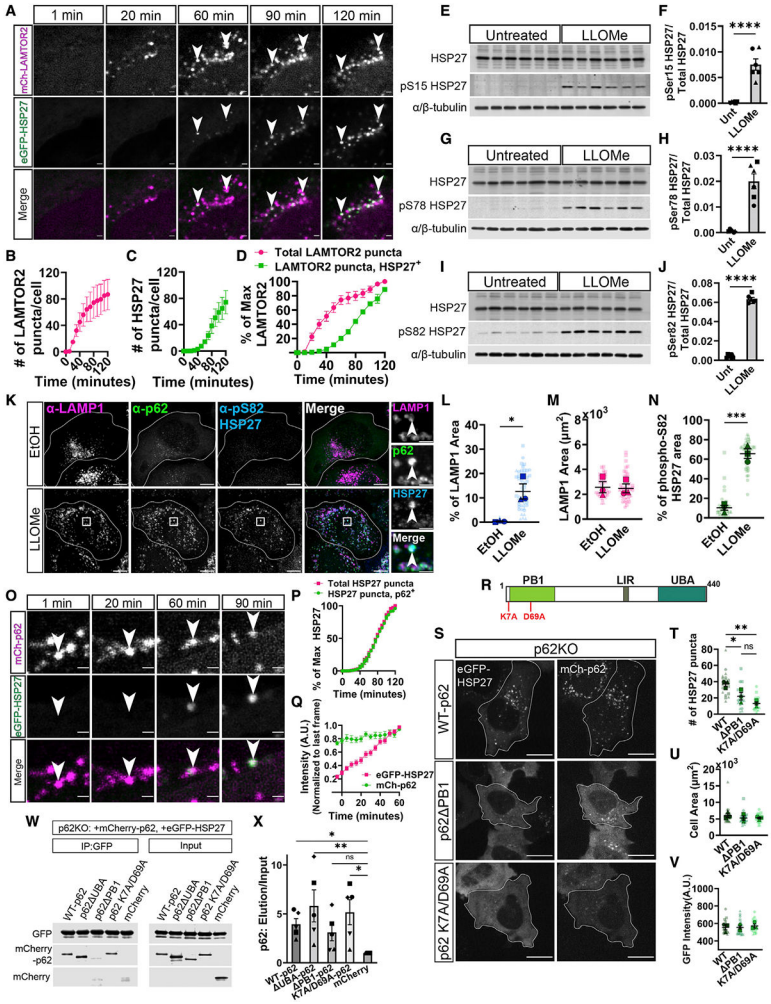

Figure 5. The small heat shock protein HSP27 and p62 dynamically interact in lysophagy

(A) Representative images of mCherry-LAMTOR2 and EGFP-HSP27 puncta following addition of 750 μM LLOMe in HeLa cells over 2 h. Arrowheads indicate co-localization over time. SBs: 2 μm.

(B) Quantification of total mCherry-LAMTOR2 puncta per cell in HeLa cells following treatment with 750 μM LLOMe (n = 7 cells).

(C) Quantification of total EGFP-HSP27 puncta per cell in HeLa cells following treatment with 750 μM LLOMe (n = 7 cells).

(D) Quantification of total mCherry-LAMTOR2 puncta and the fraction of mCherry-LAMTOR2 puncta that co-localize with EGFP-HSP27 in HeLa cells (two-way ANOVA, $p < 0.0001$, n = 7 cells).

(E) Western blot analysis of HeLa lysates for HSP27, phospho-S15 HSP27, and α/β-tubulin that were untreated (Unt) or treated with 750 μM LLOMe for 2 h.

(F) Quantification of α-phospho-S15 HSP27 band intensities normalized to α-HSP27 intensity (unpaired t test, $p < 0.0001$, n = 6 experiments).

(G) Western blot analysis of HeLa lysates for HSP27, phospho-S78 HSP27, and α/β-tubulin that were Unt or treated with 750 μM LLOMe for 2 h.

(H) Quantification of α-phospho-S78 HSP27 band intensities normalized to α-HSP27 intensity (unpaired t test, $p < 0.0001$, n = 6 experiments).
(I) Western blot analysis of HeLa lysates for HSP27, phospho-S82 HSP27, and α/β-tubulin that were Unt or treated with 750 μM LLOMe for 2 h.
(J) Quantification of α-phospho-S82 HSP27 band intensities normalized to α-HSP27 intensity (unpaired t test, $p < 0.0001$, n = 6 experiments).
(K) Representative max projections of α-LAMP1, α-p62, or α-phospho-S82 HSP27 in HeLa cells, following treatment with either EtOH or 750 μM LLOMe. White boxes indicate inset image region. Arrowheads indicate co-localization. SBs: 10 μm; insets: 2 μm.
(L) Quantification of the overlapping area from max projections between μ-phospho-S82 HSP27 and μ-LAMP1 in cells treated with EtOH or with LLOMe (unpaired t test, $p < 0.05$, n = 3 experiments. Number of cells per condition ≥ 42).
(M) Quantification of LAMP1 area from max projections in the different conditions (unpaired t test, $p = 0.8827$, n = 3 experiments. Number of cells per condition ≥ 42).
(N) Quantification of the overlapping area from max projections between α-p62 and α-phospho-S82 HSP27 in the different conditions (unpaired t test, $p < 0.001$, n = 3 experiments. Number of cells per condition ≥ 42).
(O) Representative images of mCherry-p62 and EGFP-HSP27 in HeLa cells following addition of 750 μM LLOMe over 2 h. Arrowheads indicate co-localization over time. SBs: 2 μm.
(P) Quantification of total EGFP-HSP27 puncta and the fraction of EGFP-HSP27 puncta that co-localize with mCherry-p62 over time (two-way ANOVA, $p < 0.01$, n = 4 cells).
(Q) Quantification of EGFP-HSP27 and mCherry-p62 fluorescence intensities normalized to the fluorescence at last frame analyzed. Puncta were selected if they remained in z-plane for 1 h (two-way ANOVA, $p < 0.0001$, n = 9 puncta per condition).
(R) Schematic of p62 domain architecture, highlighting K7 and D69, in the PB1 domain of p62. Alanine substitution of these residues prevents homo-oligomerization.
(S) Representative single z-plane images of EGFP-HSP27 in p62KO HeLa cells that were co-transfected with either WT, p62ΔPB1, or K7A/D69A p62. Cells were treated with 750 μM LLOMe for 2 h. Cell outlines are traced. SBs: 10 μm.
(T) Quantification of the number of EGFP-HSP27 puncta per cell (one-way ANOVA, $p_{(WT/\Delta PB1)} < 0.05$, $p_{(WT/(K7A/D69A))} < 0.01$, $p_{(\Delta PB1/(K7A/D69A)} = 0.2131$, n = 3 experiments. Number of cells per condition ≥ 21).
(U) Quantification of the cell area per cell (one-way ANOVA, $p_{(WT/\Delta PB1)} = 0.5725$, $p_{(WT/(K7A/D69A))} = 0.5899$, $p_{(\Delta PB1/(K7A/D69A)} = 0.9995$, n = 3 experiments. Number of cells per condition ≥ 21).
(V) Quantification of GFP fluorescence intensity per cell (one-way ANOVA, $p_{(WT/\Delta PB1)} = 0.9997$, $p_{(WT/(K7A/D69A))} = 0.8625$, $p_{(\Delta PB1/(K7A/D69A)} = 0.8506$, n = 3 experiments. Number of cells per condition ≥ 21).
(W) Representative Western blot demonstrating EGFP-HSP27 co-immunoprecipitation with either WT, p62ΔUBA, p62ΔPB1, K7A/D69A p62, or mCherry vector.
(X) Quantification of co-immunoprecipitation of mCherry-tagged constructs with EGFP-HSP27 (Kruskal-Wallis test, $p_{(mCherry/WT\text{-}p62)} < 0.05$, $p_{(mCherry/\Delta UBA)} < 0.01$, $p_{(mCherry/\Delta PB1)} = 0.1922$, $p_{(mCherry/(K7A/D69A))} < 0.05$, n = 5 experiments).
All error bars reflect mean ± SEM. See also Videos S4 and S5 and Figure S6.

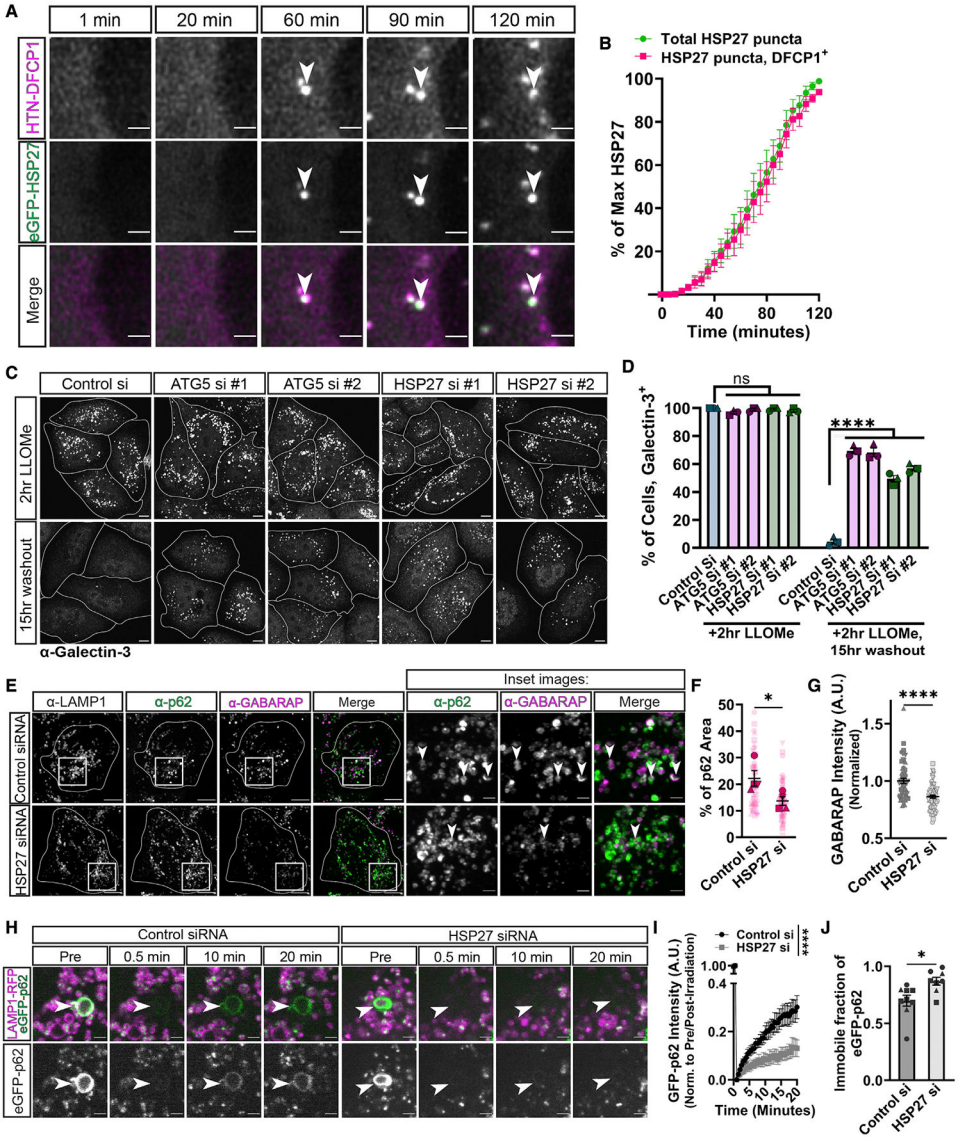

Figure 6. The small heat shock protein HSP27 regulates p62 condensates to promote lysophagy

(A) Representative images of HaloTag-DFCP1 and EGFP-HSP27 puncta in HeLa cells after addition of 750 μM LLOMe over 2 h. Arrowheads indicate co-localization. SBs: 2 μm.

(B) Quantification of total EGFP-HSP27 puncta and the fraction of EGFP-HSP27 puncta that co-localize with HaloTag-DFCP1 in HeLa cells (two-way ANOVA, $p = 0.1160$, $n = 7$ cells per condition).

(C) Representative max projections of endogenous galectin-3 flux assay. Cells were fixed immediately following LLOMe treatment or 15 h post-washout of LLOMe. Cells were transiently transfected with one of two ATG5 siRNAs, one of two HSP27 siRNAs, or a control siRNA. Cell outlines are traced. SBs: 10 μm.

(D) Quantification of the galectin-3 flux assay, indicating the fraction of cells with n > 3 galectin-3 puncta per cell (one-way ANOVA, post-LLOMe: $p_{(control/ATG5\#1)} = 0.9283$, $p_{(control/ATG5\#2)} > 0.9999$, $p_{(control/HSP27\#1)} > 0.9999$, $p_{(control/HSP27\#2)} > 0.9991$; post-washout $p_{(control/ATG5\#1)} < 0.0001$, $p_{(control/ATG5\#2)} < 0.0001$, $p_{(control/p62\#1)} < 0.0001$,

$p_{(control/p62\#2)} < 0.0001$ $p_{(ATG5\ \#1/ATG5\#2)} > 0.9999$, $p_{(HSP27\ \#1/HSP27\#2)} = 0.0571$, n = 3 experiments).

(E) Representative images of α-LAMP1, α-p62, and α-GABARAPs in HeLa cells following transient transfection of control siRNA or HSP27 siRNA (#1). White boxes indicate inset image region. Arrowheads indicate co-localization. SBs: 10 μm; insets: 2 μm.

(F) Quantification of the percentage of area of α-p62 that is occupied by α-GABARAPs (Mann-Whitney U test, $p < 0.05$, n = 4 experiments. Number of cells analyzed per condition ≥ 57).

(G) Quantification of α-GABARAPs fluorescence intensity at α-p62 segmented area across conditions (Mann-Whitney U test, $p < 0.0001$, Number of cells analyzed per condition ≥ 57).

(H) Representative images of fluorescence recovery of EGFP-p62 following photo-bleaching in cells transiently transfected with control siRNA or HSP27 siRNA (#1). Cells were treated with LLOMe for 1 h before photo-bleaching, and cells were imaged for 20 min following photo-bleaching. SBs: 2 μm.

(I) Quantification of fluorescence recovery after photo-bleaching of EGFP-p62 (two-way ANOVA, $p < 0.0001$, n = 9 puncta per condition).

(J) Quantification of the immobile fraction of EGFP-p62 across conditions (unpaired t test, $p < 0.05$, n ≥ 8 puncta per condition).

All error bars reflect mean ± SEM. See also Videos S6 and S7 and Figure S6.

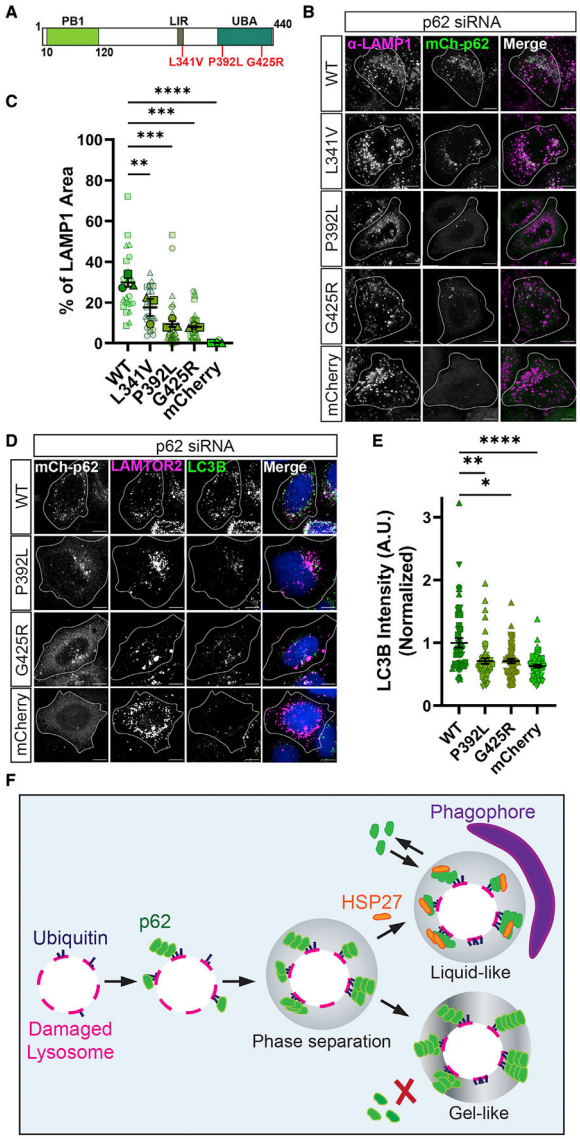

Figure 7. ALS-associated mutations in p62 perturb lysophagy

(A) Schematic of p62 domain architecture, highlighting specific ALS-associated mutations in p62 (L341V, P392L, and G425R).

(B) Representative images of α-LAMP1 in HeLa that were transiently transfected with p62 siRNA (#1) alongside either WT-p62, L341V, P392L, G425R, or mCherry vector after addition of 750 μM LLOMe for 2 h. Cell outlines were traced. SBs: 10 μm.

(C) Quantification of α-LAMP1 area overlapping with p62 area across different conditions (one-way ANOVA, $p_{(WT/L341V)} < 0.01$, $p_{(WT/P392L)} < 0.001$, $p_{(WT/G425R)} < 0.001$, $p_{(WT/mCherry)} < 0.0001$, n = 3 experiments. Number of cells analyzed per condition ≥ 22).

(D) Representative images of α-LC3B in HeLa cells that were transiently transfected with p62 siRNA (#1) alongside FLAG-LAMTOR2 and either WT-p62, P392L, G425R, or mCherry after addition of 750 μM LLOMe for 2 h. Merged channel shows LAMTOR2 and LC3B only. Cell outlines were traced. SBs: 10 μm.

(E) Quantification of normalized α-LC3B intensity at LAMTOR2 puncta across different conditions (Kruskal-Wallis test, $p_{(WT/P392L)} < 0.01$, $p_{(WT/G425R)} < 0.05$, $p_{(WT/mCherry)} < 0.0001$, $n \geq 49$ cells per condition.

(F) A model for p62-dependent lysophagy. p62 is recruited to damaged lysosomes through ubiquitin. Accumulation of p62 on damaged lysosomes results in phase separation. This phase separation of p62 is critically regulated by the small heat shock protein HSP27. HSP27 maintains the liquidity of p62 condensates, facilitating engulfment by autophagosomes.

All error bars reflect mean ± SEM. See also Figure S7.

KEY RESOURCES TABLE

REAGENT or RESOURCE	SOURCE	IDENTIFIER
Antibodies		
o/β-tubulin	Cell Signaling	Cat#:2148, RRID:AB_2288042
Alexa Fluor 488 goat anti-chicken IgG (H + L)	Invitrogen	Cat#: A11039, RRID: AB_2534096
Alexa Fluor 488 goat anti-rabbit IgG (H + L)	Invitrogen	Cat#: A11034, RRID: AB_2576217
Alexa Fluor 555 goat anti-chicken IgG (H + L)	Invitrogen	Cat#: A21437, RRID: AB_2535858
Alexa Fluor 594 donkey anti-sheep IgG (H + L)	Invitrogen	Cat#: A11016, RRID: AB_2535083
Alexa Fluor 594 goat anti-mouse IgG (H + L)	Invitrogen	Cat#: A11032, RRID: AB_2534091
Alexa Fluor 594 goat anti-rabbit IgG (H + L)	Invitrogen	Cat#: A11037, RRID: AB_2534095
Alexa Fluor Plus 647 goat anti-mouse IgG (H + L)	Invitrogen	Cat#: A32728, RRID: AB_2633277
Alexa Fluor 647 goat anti-rabbit IgG (H + L)	Invitrogen	Cat#: A31573, RRID: AB_2536183
Alexa Fluor 680 AffiniPure Goat anti-Mouse IgG light chain	Jackson Immuno	Cat#: 115-625-174, RRID: AB_2338937
FIP200	Proteintech	Cat#: 17250-1-AP, RRID: AB_10666428
FLAG M2	Sigma	Cat#: F3165, RRID: AB_259529
GABARAP (E1J4E)	Cell Signaling	Cat#: 13733, RRID: AB_2798306
GABARAP/L1/L2 (EPR4805)	Abcam	Cat#: ab109364, RRID: AB_10861928
Galectin-3	Santa Cruz Biotech	Cat#: sc-32790, RRID: AB_627657
Galectin-8	Abcam	Cat#: ab42879, RRID: AB_880161
GAPDH	Abcam	Cat#: ab9484, RRID: AB_307274
GFP	Abcam	Cat#: ab1218, RRID: AB_298911
GFP	Aves	Cat#: GFP-1020, RRID: AB_10000240
GFP-Booster ATTO 488	Chromotek	Cat#: gba488, RRID: AB_2631386
HaloTag	Promega	Cat#: G9281, RRID: AB_713650
HA-Tag (16B12) Alexa flour-594	Invitrogen	Cat#: A21288, RRID: AB_1500205
HSP27	Santa Cruz Biotech	Cat#: sc-13132, RRID: AB_627755
HSP27 pS15	Sigma	Cat#: SAB4300134, RRID: AB_10620369
HSP27 pS78	Cell Signaling	Cat#: 2405, RRID: AB_2120486
HSP27 pS82	Cell Signaling	Cat#: 2406, RRID: AB_2120485
HSP90 (C45G5)	Cell Signaling	Cat#: 4877T, RRID: AB_2233307
IRDye 680RD Donkey anti-Chicken	Li-Cor	Cat#: 926–68075, RRID: AB_10974977
IRDye 680RD Donkey anti-Guinea Pig	Li-Cor	Cat#: 926–68077, RRID: AB_10956079
IRDye 680RD Donkey anti-Rabbit	Li-Cor	Cat#: 926–68073, RRID: AB_10954442
IRDye 800CW Donkey anti-Mouse	Li-Cor	Cat#: 926–32212, RRID: AB_621847
IRDye 800CW Donkey anti-Rabbit	Li-Cor	Cat#: 926–32213, RRID: AB_621848
LAMP1	Abcam	Cat#: ab24170, RRID: AB_775978
LAMP1	R&D Systems	Cat#: AF4800, RRID: AB_1026176
LAMP1 Alexa Fluor 488	R&D Systems	Cat#: IC7985G, RRID:AB_2927803
LC3B	Abcam	Cat#: ab48394, RRID: AB_881433
LC3B	Novus Biologicals	Cat#: NB100-2220, RRID: AB_10003146
LAMTOR2/p14 (EPR14378)	Abcam	Cat#: ab183514, RRID: AB_2927804
mCherry	Abcam	Cat#: ab205402, RRID: AB_2722769

REAGENT or RESOURCE	SOURCE	IDENTIFIER
NDP52	Abcam	Cat#: ab68588, RRID: AB_1640255
OPTN	Abcam	Cat#: ab23666, RRID: AB_447598
Tau	Sigma	Cat#: MAB3420, RRID: AB_11212769
Tau	Abcam	Cat#: ab8763, RRID: AB_2927805
TAX1BP1 (EPR13287-B)	Abcam	Cat#: ab176572, RRID: AB_2927806
p62	American Research Products	Cat#: 03-GP62-C, RRID: AB_1542690
p62	Abcam	Cat#: ab56416, RRID: AB_945626
Bacterial and virus strains		
Competent E. coli	New England Biolabs	Cat#: C3040I
Chemicals, peptides, and recombinant proteins		
L-Leucyl-L-Leucine methyl ester monohydrochloride (LLOMe)	Cayman Chemicals	Cat#: 16008
Ethanol, 200 Proof	Decon Labs	Cat#: 2716
Dulbecco's Modified Eagle's Medium	Corning	Cat#: MT10-013-CV
Dulbecco's Modified Eagle's Medium	Gibco	Cat#: 11965084
Fetal Bovine Serum	HyClone	Cat#: SH3007103
GlutaMax	Thermo Fisher	Cat#: 35050061
Penicillin/streptomycin	Sigma	Cat#: P0781
Poly-L-Lysine	Sigma	Cat#: P1274
Poly-L-Ornithine	Sigma	Cat#: P3655
Neurobasal	Gibco	Cat#: 2110304
D-Glucose solution 45%	Sigma	Cat#: G8769
Sodium pyruvate	Corning	Cat#: 36017004
B27 supplement	Gibco	Cat#: 17504044
AraC	Sigma	Cat#: C6645
Minimum essential medium (MEM)	Thermo Fisher	Cat#: 11,095-072
Horse serum (heat inactivated)	Thermo Fisher	Cat#: 16,050-122
Essential 8 medium	Thermo Fisher	Cat#: A1517001
ReLeSR	Stem Cell Tech	Cat#: 05872
Accutase	Stem Cell Tech	Cat#: 07920
ROCK Inhibitor Y-27632	Selleck	Cat#: S1049
DMEM/F-12, HEPES	Thermo Fisher	Cat#: 11330032
BrainPhys Neuronal Medium	StemCell	Cat#: 05790
BDNF	PeproTech	Cat#: 450-02
NT-3	PeproTech	Cat#: 450-03
Laminin	Corning	Cat#: 354232
FuGene 6	Promega	Cat#: E269A
Lipofectamine RNAiMax	Invitrogen	Cat#: 13778150
Lipofectamine 2000	Invitrogen	Cat#: 11668030
Leibovitz's L-15 Medium	Gibco	Cat#: 11-514-064
Viral Boost Reagent	ALSTEM	Cat#: VB100
Polybrene	Sigma	Cat#: H9268
Bouin's Solution	Sigma	Cat#: HT10132

REAGENT or RESOURCE	SOURCE	IDENTIFIER
4% PFA in PBS	Thermo Fisher	Cat#: J19943.K2
Methanol	Thermo Fisher	Cat#: A545-1
Janelia Fluor 646-Halo ligand	Promega	Cat#: GA1120
Janelia Fluor Halo-TMR ligand	Promega	Cat#: G8251
Hoechst 33,342	Thermo Fisher	Cat#: H3570
ProLong Gold Antifade mountant	Life Technologies	Cat#: P36930
Bafilomycin A1	Sigma	Cat#: SML1661
Tween 20	Bio-Rad	Cat#: 17065
Halt Protease and Phosphatase Inhibitor Cocktail	Thermo Fisher	Cat#: 78442
10% SDS	Invitrogen	Cat#: 15,553-035
Tris Base	Thermo Fisher	Cat#: BP142-1
NaCl	Thermo Fisher	Cat#: BP358-1
KCl	Sigma	Cat#: P9541
EDTA	Invitrogen	Cat#: 15,575-038
NP-40	Sigma	Cat#: I3021
Triton X-	Sigma	Cat#: X100
Glycerol	Invitrogen	Cat#: 15,514-011
Phenylmethanesulfonyl Fluoride	Sigma	Cat#: P7626
TAME	Sigma	Cat#: 172104
Leupeptin	Sigma	Cat#: 11017128001
Pepstatin-A	Sigma	Cat#: EI10
$NaPO_4$	Thermo Fisher	Cat#: BP330
KH_2PO_4	Thermo Fisher	Cat#: P285
Sucrose	Thermo Fisher	Cat#: BP220
Critical commercial assays		
BCA Protein Assay Kit	Thermo Fisher	Cat#: 23225
MycoAlert Detection Kit	Lonza	Cat#: LT07
Plasmid Maxi Kit	Zymo research	Cat#: D4202
Experimental models: Cell lines		
HeLa-M	Andrew Peden, Cambridge Institute for Medical Research	N/A
HeLa WT	Richard Youle, National Institutes of Health	N/A
p62KO HeLa	Richard Youle, National Institutes of Health	N/A
pentaKO HeLa	Richard Youle, National Institutes of Health	N/A
HEK293	Gibco	Cat#: R70507
Experimental models: Organisms/strains		
Rat: Dissociated hippocampal neuron cultures from embryonic day 18 rat brains (Sprague Dawley)	University of Pennsylvania, Neuron Culture Service Center	N/A
Mice: C57BL/6NTac WT	Taconic	Model #B6

REAGENT or RESOURCE	SOURCE	IDENTIFIER
Oligonucleotides		
p62 siRNA #1	Horizon Discovery	Cat#: J-010230-05
p62 siRNA #2	Horizon Discovery	Cat#: J-010230-07
ATG5 siRNA #1	Horizon Discovery	Cat#: J-004374-09
ATG5 siRNA #2	Horizon Discovery	Cat#: L-004374-00
HSP27 siRNA #1	Horizon Discovery	Cat#: L-005269-00
HSP27 siRNA #2	Horizon Discovery	Cat#: J-005269-06
Recombinant DNA		
pEGFP-C2-WT HSP27	Voss et al.[92]	Addgene plasmid: 17,444
pEGFP-C2-3XSA (S15D/S78D/S82) HSP27	This paper	N/A
pEGFP-C2-3XSD (S15D/S78D/S82) HSP27	This paper	N/A
pEGFP-C1-Galectin-3	This paper	N/A
pFN21A-HaloTag-TAX1BP1	Promega	Catalog#: FHC02883
pEGFP-C3-TAX1BP1	Moore and Holzbaur,[93]	N/A
pEGFP-C1-NBR1	Peter Kim Lab, The Hospital for Sick Children, University of Toronto	N/A
pEGFP-C1	ClonTech	Cat#: V012024
pHaloTag-N1	Promega	Cat#: G7721
pHaloTag-DFCPI	Stavoe et al.[94]	N/A
pHaloTag-WIPI2B	Stavoe et al.[94]	N/A
pLAMP1-KillerRed (EGFP bb)	This paper	N/A
pLAMP1-HTC	This paper	N/A
pTagBFP-N-LAMP2	This paper	N/A
pLJC5-Tmem192-3xHA	Abu-Remaileh et al.[41]	Addgene plasmid: 102,930
pRK5-FLAG-LAMTOR2	Bar-Peled et al.[95]	Addgene plasmid: 42,330
pmCherry-LAMTOR2	This paper	N/A
pmCherry-LC3B	Fu et al. 2014[96]	N/A
pHaloTag-LC3B	This paper	N/A
pmCherry-C1	Sascha Martens, University of Vienna	N/A
pmCherry-C1-WT-p62	Sascha Martens, University of Vienna	N/A
pmCherry-C1-p62ΔUBA	Sascha Martens, University of Vienna	N/A
pmCherry-C1-p62ΔPB1	Sascha Martens, University of Vienna	N/A
pmCherry-C1-p62 LIR^{AAAA}	Sascha Martens, University of Vienna	N/A
pmCherry-C1-p62 K7A/D69A	Sascha Martens, University of Vienna	N/A
pmCherry-C1-p62 G425R	This paper	N/A
pmCherry-C1-p62 L341V	This paper	N/A
pmCherry-C1-p62 P392L	This paper	N/A
pEGFP-C1-hWT-p62	This paper	N/A

REAGENT or RESOURCE	SOURCE	IDENTIFIER
pMXs-puro-eGFP-p62	Itakura et al.[97]	Addgene plasmid: 38,277
pHaloTag-p62	This paper	N/A
pPGK-LAMP1mNeon	Michael Ward, National Institutes of Health	N/A
pCMV-VSV-G	Bob Weinberg, Whitehead institute	Addgene plasmid: 8454
psPAX2	Didier Trono, EPFL	Addgene plasmid: 12,260
Software and algorithms		
Prism version 9.2.0	Graphpad	N/A
Fiji Image Analysis	ImageJ	https://imagej.net/software/fiji/
Volocity	PerkinElmer	https://www.perkinelmer.com/
Visiview	Visitron Systems	https://www.visitron.de/
Ilastik	Berg et al.[98]	https://www.ilastik.org/
Other		
Glass-bottom tissue culture dishes	MatTek	Cat#: P35G-1.5-20-C
Glass coverslips	Electron Microscopy Science, Fisher	Cat#: 50-948-975
DynaBeads Protein G	Thermo Fisher	Cat#: 10003D
Pierce Anti-HA Magnetic beads	Thermo Fisher	Cat#: 88837
Immobilon-FL PVDF membranes	Sigma	Cat#: IPFL00010
TrueBlack WB Blocking Buffer	Biotum	Cat#: 23013
EveryBlot Blocking Buffer	Bio-Rad	Cat#: 12010020